

https://dspace.org/

The dosimetric impact of setup errors in image guided radiotherapy

Maabane, Berry

2025
University of the Witwatersrand, Johannesburg
https://hdl.handle.net/10539/50319
Maabane, Berry. (2025). The dosimetric impact of setup errors in image guided radiotherapy. [Master's dissertation, University of the Witwatersrand, Johannesburg]. WIReDSpace. https://hdl.handle.net/10539/50319

Downloaded from a DSpace repository. https://dspace.org/

The dosimetric impact of setup errors in image-guided radiotherapy



by

BERRY MAABANE

STUDENT NUMBER: 1661515

A research report submitted to the Faculty of Science, University of the Witwatersrand, Johannesburg, in fulfilment of the requirements for the degree of Master of Science (Medical Physics)

Supervisor: Dr. S. Ngcezu

Co-supervisor: Sekone Lehlabile Appreciate

2025

Declaration

I Berry Maabane affirm that this research report, submitted to the University of the Witwatersrand in fulfilment of the requirements for the degree of Master of Science in Medical Physics, is my original work. It has not been submitted before for any degree or examination at this or any other University.

The University of the Witwatersrand Human Research Ethics Committee granted approval of ethics clearance certificate of reference No. M240148 for this work on the 6th of May 2024.



(Signature of candidate)

___20_____day of_____March_____20_____25_____in____Witbank_____

Dedication

To

My mother **Julia Motsamai Soki** and my sisters. This achievement would not have been possible without your unwavering support, love, guidance, encouragement , and belief in me.

Acknowledgement

My special thanks to my supervisors Dr. Sonwabile Ngcezu and Lehlabile Appreciate Sekone, for their invaluable input, patience, suggestion, guidance, and encouragement throughout this research project. I would like to thank the staff and interns at Charlotte Maxeke Johannesburg Academic Hospital for their assistance with the operation of the equipment and guidance. I am grateful to the institution for allowing me to use their facility to conduct my research. I am deeply thankful to the Council of Scientific and Industrial Research (CSIR) and Tirisano Trust Fund for their massive assistance in funding my studies.

Glossary

2D	Two Dimensional
3D	Three Dimensional
AMFPI	Active Matrix Flat Panel Imagers
ANT	Anterior
ART	Adaptive Radiation Therapy
CBCT	Cone Beam Computed Tomography
CMJAH	Charlotte Maxeke Johannesburg Academic Hospital
CRT	Conformal Radiation Therapy
CT	Computed Tomography
CTV	Clinical Target Volume
DVH	Dose Volume Histogram
DRR	Digitally Reconstructed Radiographs
EPID	Electronic Portal Imaging Devices
GTV	Gross Tumour Volume
Gy	Gray
ICRU	International Commission on Radiation Units and Measurements
IGRT	Image-guided radiation Therapy
IMRT	Intensity Modulated Radiation Therapy
IMPT	Intensity Modulated Proton Therapy
INF	Inferior
ITV	Internal Target Volume
KV	Kilovoltage
LINAC	Linear Accelerator
Lt	Left
MC	Monte-Carlo
MRI	Magnetic Resonance Imaging
MU	Monitor Units
MV	Megavoltage
NTCP	Normal Tissue Complication Probability
OAR	Organs at Risk
PET	Positron Emission Tomography

POST	Posterior
PSQA	Patient Specific Quality Assurance
PTV	Planning Target Volume
QA	Quality Assurance
RT	Radiation Therapy
Rt	Right
RVS	Record and Verify System
SIB	Simultaneous Integrated Boost
SRS	Stereotactic Radiation Surgery
SRT	Stereotactic Radiation Therapy
SUP	Superior
TCP	Tumour Control Probability
TPS	Treatment Planning System
VMAT	Volumetric Modulated Arc Therapy

Table of Contents

Declaration i

Dedication ii

Acknowledgement iii

Glossary iv

Table of Contents vi

List of figures 1

List of tables 3

Abstract 4

1. Introduction 6

1.1. Background 6

1.2. Problem statement 8

1.3. Motivation of the study 9

1.4. Research questions. 10

1.5. Aims and objectives 11

1.6. Outline of the Research Report 11

2. Theoretical Background 12

2.1. Linear accelerator (LINAC) 12

2.2. Electronic portal imaging devices (EPIDs) 13

2.3. Digitally Reconstructed Radiographs 15

2.4. 3D Cone Beam Computed Tomography 16

2.5. Image registration 19

2.6. IMRT Technique 19

2.7. VMAT Treatment Technique 20

2.8. Target Volumes and Organs at risk 22

2.9. Setup Errors 24

2.9.1. Systematic errors 24

2.9.2. Random errors 24

2.10. Literature Review 25

3. Materials and Methodology 27

3.1. Materials 27

3.1.1. Anthropomorphic Phantom: CIRS Shane phantom 28

3.1.2. Computed Tomography: The AquilionLB V6.6 system 29

3.1.3. The Treatment Planning System: Monaco 30

3.1.4. Patient-Specific Quality Assurance System: Octavius® 4D 30

3.1.5. The Record and verify System: MOSAIQ. 31

3.2. Methodology 32

3.2.1. Imaging 32

3.2.2. Planning 33

3.2.3. Patient-Specific Quality Assurance 35

3.2.4. Patient selection 37

3.2.5. Positional Shifts and Dose calculation 38

4. Results analysis and Discussion 41

4.1. Translational shifts on a SHANE phantom plan 41

4.1.1. PTV Evaluation 41

4.1.2. OARs Evaluation 44

4.2. Patient Data Shifts: Dosimetric Impact on PTV 48

4.3. Patient Data Shifts: Dosimetric Impact on OAR 52

4.5. OCTAVIUS 4D dose evaluation 60

5. Conclusion 62

6. References 65

List of figures

Figure 1: Linear accelerator integrated with CBCT system. 13
Figure 2: EPIDs. Image accessed from ELEKTA-iViewGT. 14
Figure 3: DRRs are produced through the simulations of X-ray propagation within a volumetric CT. 15
Figure 4: CBCT geometry schematic illustration. 18
Figure 5: 3D view of VMAT treatment. 21
Figure 6: Diagram illustration of ICRU report 50, 62, and 83 volumes. 22
Figure 7: Schematic illustration of systematic errors. 25
Figure 8: SHANE phantom. 28
Figure 9: Canon AcquilionLB V6.6 Computed Tomography. 29
Figure 10: The OCTAVIUS 4D system. 31
Figure 11: CIRS Shoulder, Head and Neck Shane phantom. The treatment position of the phantom was head first supine on the CT simulation. 33
Figure 12: CT scan of the CIRS Shoulder, Head and Neck Shane phantom illustrating the delineated volumes in coronal view. 34
Figure 13: Illustrates the recalculation of the QA plans with shifts on the treatment planning system while varying the isocenter position. 35
Figure 14: The 4D phantom in isocentric position on the treatment table. 36
Figure 15: Illustration of how positional shifts were introduced through couch movement in lateral, longitudinal, and vertical directions. 37
Figure 16: Transverse view of VMAT plan with at least two full rotation beams (arcs). 38
Figure 17: Illustrates how the positional shifts of the beam were introduced on the copied plans and how they were recalculated. 39
Figure 18: Three PTVs; PTV_7000 (red), PTVn1_6000 (green), and PTVn2_5400 (blue), plotted against the translational shifts; (a) lateral, (b) longitudinal, and (c) vertical along x-axis. 42
Figure 19: Mean dose of all critical organs plotted again the translational shifts; (a) lateral shifts, (b) longitudinal shifts, and (c) vertical shifts. 45
Figure 20: Dose response of PTV to lateral shifts in VMAT radiotherapy plan. 48
Figure 21: Dose response of PTV to vertical shifts in VMAT radiotherapy plan. 49
Figure 22: Dose response of PTV to vertical shifts in VMAT radiotherapy plan. 50

Figure 23: Hotspots (D2%<69.3 Gy) for translational shifts; Lateral, longitudinal, and vertical. 51
Figure 24: Impact of lateral shifts on mean dose of surrounding critical cochlear organs. 52
Figure 25: Impact of lateral shifts on mean dose of surrounding critical parotid glands. 53
Figure 26: Impact of lateral shifts on maximum dose of surrounding eyes and lenses critical organs. 54
Figure 27: Impact of lateral shifts on maximum dose of surrounding spinal cord, brainstem, and brain critical organs. 54
Figure 28: Impact of longitudinal shifts on mean dose of surrounding critical cochlear organs. 55
Figure 29: Impact of longitudinal shifts on mean dose of surrounding critical parotid glands. 56
Figure 30: Impact of longitudinal shifts on maximum dose of surrounding critical organs, including eyes and lenses. 56
Figure 31: Impact of longitudinal shifts on maximum dose of surrounding critical organs, including spinal cord, brainstem, and brain. 57
Figure 32: Impact of vertical shifts on mean dose of surrounding cochlear critical organs. 58
Figure 33: Impact of vertical shifts on mean dose of surrounding critical parotid glands. 58
Figure 34: Impact of vertical shifts on maximum dose of surrounding eyes and lenses critical organs. 59
Figure 35: Impact of vertical shifts on maximum dose of surrounding critical organs like spinal cord, brainstem, and brain. 59
Figure 36: Impact of translational shifts; lateral (red), longitudinal (green), and vertical (blue) on gamma passing rate in PSQA. 60

List of tables

Table 1: Dose constraints for Nasopharynx cancer 40
Table 2: The established shift tolerance of the PTVs for Shane phantom. 44
Table 3: The established shift tolerances of both parotid glands, spinal cord, and brainstem across all directions for Shane phantom. 47
Table 4: Established shift tolerances obtained from the calculations based on PTV tolerances 50
Table 5: Established shift tolerances obtained from measured PSQA data. 61
Table 6: The summary of verification recommendations at CMJAH and literature comparison. 64

Abstract

Aim

This study aimed to contribute to clinical implementation of imaging protocols in Image-Guide Radiotherapy (IGRT) by evaluating the impact of positional shifts on the dose distribution and target coverage in Volumetric Modulated Arc Therapy (VMAT) for nasopharynx cancer. The study focused on understanding the dosimetric impact of these shifts on Planning Target Volumes (PTVs) and Organs at Risks (OARs). In radiotherapy, the adoption of advanced treatment techniques made possible by technological advancements demands higher levels of setup accuracy, necessitating standard operating procedures in IGRT and associated quality assurance (QA) program that enhance patient plan verification and treatment accuracy without compromising treatment efficacy.

Methodology and Materials

The measurement were performed on anthropomorphic CIRS Shoulder, Head and Neck (SHANE) phantom, simulating patient anatomy to assess the effect of positional shifts in VMAT plans for nasopharyngeal cancer. In accordance with IAEA and QUANTEC guidelines, a VMAT plan with at least two full rotation beams (arcs) was created with a dose prescription of 70 Gy distributed in 35 fractions, giving 2.0 Gy per fraction to PTV_7000. Corresponding copied plans from the original VMAT were developed by introducing positional shifts to the isocenter in all directions. These copied plans were recalculated and evaluated in the Elekta Monaco 6.1.2.0 treatment planning system (TPS) using plan Dose-Volume Histogram (DVH) data to analyze the dosimetric impact. For Patient Specific Quality Assurance (PSQA), the Octavius 4D phantom with 1500-chamber array was employed to assess the impact of these positional shifts on dose distribution using VeriSoft software (version 7.2). The measured dose distribution resulting from these translational shifts was compared with the planned dose distribution from TPS using Gamma analysis method. Data from the DVH analyses and gamma passing rates were employed to determine shift tolerances, which were then compared to literature-based tolerances.

Results

The study investigated the impact of positional shifts on dose distribution in VMAT for nasopharyngeal cancer, focusing on maintaining optimal PTV coverage and sparing OARs. Results showed that translational shifts greater than ±2 mm reduces the PTV dose coverage, with the $D_{98\%} > 62.7$ Gy criterion failing beyond ±2 mm and decreasing by up to 50% of the initial PTV dose coverage at maximum shifts (±20 mm), potentially compromising treatment efficacy. DVH statistics showed that longitudinal and vertical shifts, particularly with inferior and posterior shifts, resulted in decrease of PTV dose coverage by up to 70% and 40%. Hot spots increase with lateral, longitudinal, and vertical shifts, posing the risks of unintended dose escalation. Dose distribution to OARs, including spinal cord, brainstem, brain, and parotid glands, varied depending on positional shifts, increasing risk of overdosing these critical organs. PSQA further highlighted the importance of accurate and precise patient positioning, with lateral and vertical shifts resulting in gamma passing rate failure, and established a shift tolerances of 4-6 mm. The results highlight the critical need for imaging protocols to account for setup errors to ensure target conformity, optimal dose delivery, and treatment efficacy.

Conclusion

The dosimetric impact of positional shifts in nasopharynx patients undergoing VMAT radiotherapy and Shane phantom were investigated. The study showed that even minor shifts effect the dose coverage of the OARs and PTV, potentially compromising patient safety and treatment efficacy. The study emphasized the importance of accurate patient positioning, strict adherence to the established shift tolerances (±2 mm), and verification techniques such as daily or weekly IGRT (e.g., CBCT), PSQA, and adaptive planning. Overall, the study emphasize a rigorous patient position verification process and regular use of QA tools like the Octavius® 4D system, as well as adherence to established shift tolerances to maintain effective dose delivery, particularly in sensitive regions like nasopharynx, where proximity of critical organs requires accurate and precise treatment planning.

Chapter 1

1. Introduction

1.1. Background

Historically, x-ray imaging have been critical in guiding radiation therapy (RT) (O'Connor A., 1949). Initially, the same kilovoltage (kV) radiation source was utilised both for imaging and therapeutic purposes in cancer therapy (Breitkreutz, et al., 2020). The concept of image guidance in RT has experienced substantial development over the years. In recent years, image guidance has gained significant momentum because of commercial availability of advanced online volumetric imaging systems or technologies. These technologies enable near real-time verification of treatment delivery, thereby increasing the precision of RT. Modern image-guided radiotherapy (IGRT) emphasizes its application on real time imaging for setup correction and treatment verification (Ling, et al., 2006). IGRT utilizes sophisticated imaging modalities, including computed tomography (CT), positron emission tomography (PET), and magnetic resonance imaging (MRI) to precisely localize the mass and surrounding normal organs prior to each treatment session. This precision allows for optimal adjustment of treatment beams, ensuring optimal radiation delivery to cancer cells while minimizing impact on surrounding healthy organs (Jaffray & Wong, 2013). IGRT integrates image guidance at various stages, including patient data acquisition, simulation, treatment planning, patient positioning, and target localisation before and during therapy.

In modern radiotherapy practice, a range of malignant and benign cancers are managed in clinics the world over, including Nasopharyngeal cancer. Nasopharyngeal carcinoma is arises from the epithelial cells within the nasopharynx. RT serves as the primary treatment for non-metastatic nasopharyngeal carcinoma due to the tumour's high radio sensitivity and the nasopharynx's intricate anatomy (Zhu, et al., 2023; Ng, et al., 2022). In recent decades, advancements in RT have facilitated the development of more effective treatment approaches. Three dimensional conformal radiation therapy (3D-CRT) and Intensity modulated radiation therapy (IMRT) have replaced conventional two-dimensional (2D) RT. Studies have shown that IMRT enhances tumour control and reduces adverse effects such as hearing loss, xerostomia, and temporal lobe neuropathy in comparison to conventional RT (Zhou, et al., 2024; Du, et al., 2019).

IGRT has significantly improved patient positioning accuracy, therefore increasing confidence in the adequacy of dose coverage to the tumour and, in many cases, sparing healthy tissues (Li, et al., 2011). In recent years, the widespread use of IGRT has expanded the limits of maximizing the target dose while minimizing the exposure to normal organs. Acquisition of functional and anatomical data from various medical imaging modalities, leveraging the unique clinical attributes of each imaging modality, is the principle for the success of IGRT. The primary objective of IGRT is to facilitate online treatment corrections based on the imaging data taken prior to or during RT. IGRT correction strategies can be categorized into offline and online approaches. Offline IGRT involves corrections and verification applied to subsequent sessions, while online IGRT refers to adjustments made when the patient still on the treatment couch, allowing immediate correction.

An online strategy for IGRT involves the acquisition, verification and corrections using images prior to a treatment session to correct for random and systematic errors due to patient positioning errors and patient anatomy changes with a fraction or multiple fractions. Online imaging frequency depends on the treatment site and the anticipated error magnitude. For treatment sites with substantial daily shifts, like the thorax, abdomen, and pelvis, or where even minor shifts can have a great impact on the dose distribution in adjacent critical structures, such as paraspinal and intracranial tumours near optic structures, generally, daily imaging could be recommended (Goyal & Kataria, 2014). Online corrections analysis shows that errors are most prevalent in the thorax, followed by the abdomen and pelvis, while the head and neck regions have the lowest error frequency (Kataria, et al., 2011). On the other hand, an offline approach entails capturing images before treatment delivery and comparing them to a reference image later to pinpoint and reduce individual systematic setup (Bel, et al., 1993).

Accurate verification and correction of positioning have become crucial in modern RT for the care of cancer patients. This shift is predominantly driven by the necessity to limit the volume exposure to high doses of RT, improve treatment accuracy, and reduce radiation toxicity on healthy tissues. Imaging in RT is important for planning and treatment delivery, particularly in cases where the treatment target is deep-seated and visual verification is not possible. Examples of traditional radiation approaches include anatomical surface markers and radiologic association with two-dimensional (2D) imaging, such as fluoroscopic imaging or port film (Goyal & Kataria, 2014). One of the distinguishing features of IGRT is its ability to ensure accurate tumour localisation. To account for treatment uncertainties and ensure optimal target

coverage, a planning target volume (PTV) margin is added around the tumour. This procedure enables precise delivery of therapeutic doses to the tumour while minimizing exposure to healthy adjacent tissues.

In recent decades, significant advances in precision and effectiveness have been observed in radiation oncology, largely due to advancements in treatment planning. This includes the use of advanced computer techniques to deliver fluence-modulated beams that include photon and particle-based radiation. A prominent example is the introduction of the IMRT technique in the clinic, which enables precise dose distribution to the treatment volume while reducing exposure to organs at risk (OARs) (Bortfeld, 2006). Modern external beam RT treatments, including IMRT, stereotactic radiotherapy (SRT), volumetric modulated arc therapy (VMAT), and stereotactic radiosurgery (SRS), have significantly reduced safety margins around the target volume (Goyal & Kataria, 2014). These developments allow the administration of reduced radiation doses to healthy tissues while still ensuring treatment delivery to cancerous regions.

The current study, given the essential role of RT in cancer treatment, aims to map out the dosimetric consequences that can result from both random and systematic positional errors during treatment delivery for patients treated for Nasopharyngeal carcinoma. Our focus is on the dosimetric consequences of setup errors. In this study, Elekta Monaco treatment planning system (TPS) was employed for quantification of dosimetry, and the Elekta Versa HD linear accelerator (Linac) was utilized deliver VMAT treatment plans to the Octavius® 4D system for quality assurance (QA) and dosimetric evaluation.

1.2. Problem statement

Charlotte Maxeke Johannesburg Academic Hospital (CMJAH) has introduced new technologies, such as the Elekta Versa HD Linac. The introduction of these new RT technologies has led to the adoption of advanced treatment technique techniques that necessitates precise patient positioning and accurate image guidance in order to achieve optimal treatment delivery. However, setup errors in RT significantly affect the dose distribution, which results in underdosing of the PTV and overdosing of the surrounding OARs. These errors compromise treatment efficacy, showing the need for local protocol recommendations or development for imaging, planning, and verification.

Optimizing IGRT is important to account for setup errors and to ensure accurate treatment delivery, enhanced patient safety, and overall improved effectiveness of RT. Here are some challenges that may arise when IGRT is not appropriately optimised:

- Reduced tumour targeting accuracy
- Increased radiation exposure
- Potential overdose of healthy organs

Research has demonstrated that IGRT accuracy or precision impact on overall survival and treatment outcome, emphasizing the importance of enhancing accuracy and precision (FitzGerald, et al., 2008). Advances in RT planning and delivery techniques, including 3D CRT, proton/neutron therapy, and IMRT, enables much better dose conformity, steeper dose gradient, and higher doses per fraction. As a results, the impact of setup errors becomes more pronounced (Hartford, et al., 2009).

1.3. Motivation of the study

The aim of RT is to eradicate the tumour without endangering the adjacent healthy organs. However, the radiation doses needed to attain sufficient tumour control often exceed the dose tolerated by normal healthy tissue or organs in most clinical situations, particularly when large volumes of adjacent organs are exposed to radiation. The core principle of radiation oncology and the main challenge is the balance between the radiation dose-response relationship for tumour control and the probability of normal tissue toxicity (Hall & Giaccia, 2019).

Delivering RT with high precision in the absence of periodic image guidance could potentially have more negative consequences than treating large volumes to counteract setup inaccuracies. IGRT allows for evaluation of the patient's model geometry accuracy throughout the treatment administration. It offers a technique for identifying anatomical deviations from the original treatment plan and update dosimetric assumptions based on this information. Strategies for correction encompass daily patient repositioning to accurately align with the initial treatment plan. Additionally, treatment delivery can be recalculated in real time during each fraction to accommodate changes in the patient′s position. This approach, called Adaptive Radiotherapy (ART), involves reassessing treatment plan and accounting for discrepancies between the patient's actual anatomy on a specific day and the initially established treatment plan (Wu, et al., 2011).

Accurate RT technology requires minimizing the impact of setup errors or positioning errors. A major challenge in improving treatment accuracy is addressing these positional errors. In RT, the margins from the clinical target volume (CTV) to the PTV are largely determined by the size of these external errors (Nijkamp, et al., 2008). Changes in anatomy of the patient, such as tumour growth or shrinkage, can occur during treatment, or patients may experience detrimental effects like weight loss, weight gain, pain, or fatigue. These factors must be carefully monitored, as they can seriously affect the patient's positioning and, consequently, the treatment delivery accuracy (JAFFRAY, et al., 2005). Without periodic image guidance, the risk of inaccurate tumour targeting increases. Tumours can shift or undergo changes in shape and size over time due to different factors, including changes in patient anatomy, respiratory motion, and organ motion. Relying solely on the initial imaging increases the chance of missing the tumour or irradiating surrounding healthy tissues, which can reduce the efficacy of the treatment and potentially harm the surrounding organs. The impact of setup errors in radiation oncology is investigated in several studies to enhance the accuracy and quality of the cancer therapy. The distribution of radiation doses to the targeted area and surrounding OARs is usually the focus of these studies, which look at even minor changes in patient motion. One study investigated the effects of positioning errors in breast cancer with VMAT and fiend-in-field (FiF) delivery techniques (Zhao, et al., 2020).

This research addresses the importance of reducing setup errors in RT. These setup errors can compromise the balance between the tumour control probability (TCP) and normal tissue complication probability (NTCP). Using the TPS, this research aims to evaluate and quantify the dosimetric impact of positional shifts, providing information about how setup errors affect the distribution of dose within planned treatment volume and OARs. The results will contribute to the derivation of appropriate positional limits and help reduce normal tissue toxicity, improve treatment accuracy, and improve RT outcomes.

1.4. Research questions.

This study aims to address the following key challenges and questions:

- What is the dosimetric impact of translational shifts on PTV coverage in VMAT treatment for nasopharyngeal cancer?
- How do positional shifts affect the dose distribution to OARs in VMAT technique for head and neck cancer patients?

- What is the correlation between the magnitude of translational shifts and the hot spots within the PTV?
- What is the maximum tolerable positioning error in the nasopharynx before clinically significant dosimetric deviations occur?

The aim of this research is to enhance patient outcomes and advance cancer therapy by contributing to the continuous advancement of IGRT and RT techniques, emphasizing patient centered precision medicine.

1.5. Aims and objectives.

The radiation oncology department in CMJAH requires new clinical protocols that address the following objectives:

- Optimum imaging protocols in the RT department will benefit patient verification and treatment.
- Setting up clinical protocol development in IGRT and the associated QA recommendations.

1.6. Outline of the Research Report

Chapter One introduces IGRT and emphasizes its importance in addressing setup errors in RT. The purpose, motivation, aims, and some research questions to be addressed in this study are covered in the introduction.

Chapter Two reviews the literature on various techniques in IGRT. The advantages and disadvantages of these IGRT techniques are discussed in detail in this chapter. The definition and different types of setup errors are also discussed.

Chapter Three outlines the materials and methodology followed in this study to evaluate the impact of setup errors in treatment planning. It also details the use of the Octavius 4D phantom, clearly explaining the tools and procedures used throughout the research.

Chapter Four provides the results of the measure data on setup errors and offers a detailed discussion of the findings.

Chapter Five gives the conclusion drawn from the research and provides recommendations based on the results obtained.

Chapter 2

2. Theoretical Background

2.1. Linear accelerator (LINAC)

Decades of technological advancement have led to the development of the contemporary microwave electron Linac, referred to as an electron linac, with diverse applications in medicine, industry, and science. This sophisticated instrument integrates high power pulsed microwave production, electronics, advanced vacuum technology, as well as metal forming and assembly (LAPOSTOLLE & SEPT1ER, 1970). In RT, the utilization of second and third generation electron linacs is widespread for treating cancer, offering enhanced output, broader treatment fields, simplicity, dependability and the option of photon or electron irradiation. Higher energies provided by electron linacs prove advantageous due to their increased tissue penetration capabilities, enabling the treatment of deep-seated tumours while ensuring better skin protection. With a small focal spot, the beam can be defined precisely. Additionally, Linacs are compact and can be easily converted into rotational therapy units. Cancer therapy is the most common use of electron linacs, both in terms of societal significance and the number of accelerators currently in use, which exceeds 800 (KARZMARK & PERING, 1973; ALMOND, 1975).

Modern Linacs such as the Elekta Versa HD are integrated with two distinct imaging modalities: a kV x-ray imager and a megavoltage (MV) electronic portal imaging device (EPID). The kV x-ray imaging system comprises a conventional x-ray tube affixed to the gantry, paired with a flat-panel image detector positioned apposite it. The MV EPID also features its own flat-panel image detector. As illustrated in Figure 1, both flat-panel image detectors are comprises 256 x 256 solid-state detectors made up of amorphous silicon (a-Si) photodiodes. The on-board kV imaging system of the Elekta Versa HD enables integrated cone beam computed tomography (CBCT) and fluoroscopy. The x-ray tube, affixed to a retractable arm, is positioned 90 degrees from the central axis of the linac beam. Flat panel area detectors positioned opposite the x-ray tube generate the image. KV-CBCT captures planar projection images from various angles while the gantry rotates 180 degrees or more. The computer uses a filtered back-projection (FBP) algorithm to reconstruct 3D volumetric images from these multiple radiographs (Feldkamp, et al., 1984).



Figure 1: Linear accelerator integrated with CBCT system. Image courtesy of CMJAH

2.2. Electronic portal imaging devices (EPIDs)

EPIDs were first introduced in clinical settings in the 1990s. By the early 2000s, EPIDs had become standard onboard imaging systems for all modern linacs, as illustrated in Figure 2. (Antonuk, et al., 1993; Antonuk, et al., 1996). The task group 58 (TG-58) report (Herman, et al., 2001) emphasized that the underuse of EPIDs in the United States and the lack of widespread clinical applications were primarily due to poor image quality. However, EPIDs were still preferred over film, as they provided online feedback and quantitative data. EPIDs found applications in various areas including treatment QA of treatment (Luchka, et al., 1996), in vivo dosimetry measurements during radiation delivery (Essers, et al., 1996; Kirby & Williams, 1995), and verification for sophisticated delivery techniques such as IMRT. Additionally, the report briefly mentioned the potential for EPIDs in advanced applications but did not provide further details.

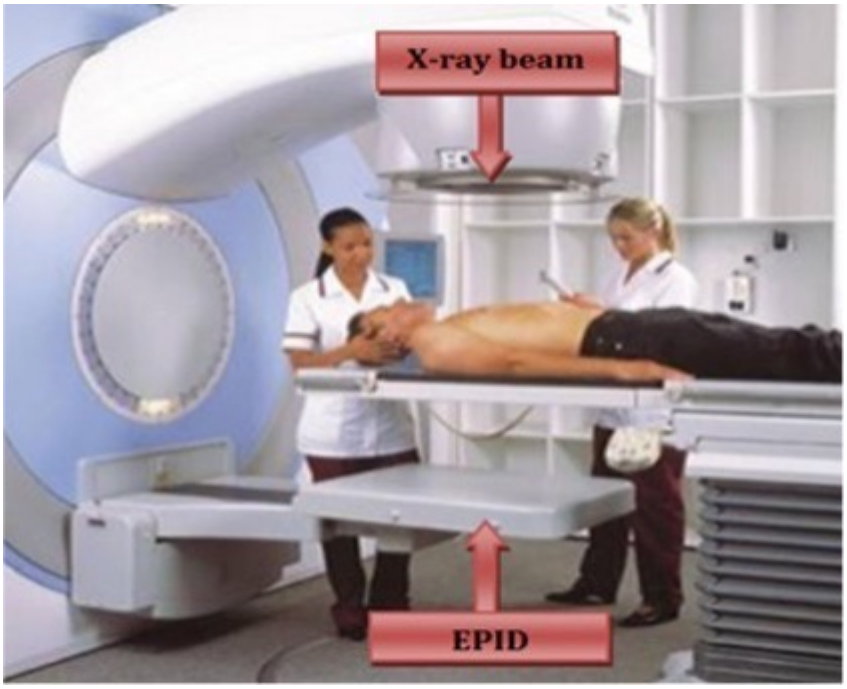

Figure 2: EPIDs. Image accessed from ELEKTA-iViewGT.

Although portal images were traditionally acquired with film, EPIDs are becoming an increasingly popular technique for capturing them. The benefits of using an EPID include instant access to images without the need for expensive and time-consuming film development. Additionally, the digital nature of EPID images enables easy access over a computer network, facilitating image matching and image processing. Initially, the disadvantages of EPIDs included poor image quality and their bulky design because of poor differential x-ray attenuation and significant Compton scatter, leading to reduced subject contrast and a less sharp image (El-Shahat, et al., 2023). However, modern technological advancements have significantly improved both factors. Despite these improvements, there are still concerns regarding the considerable amount of work involved in the installation, implementation and specification of an EPID system (Herman, et al., 2001). Nonetheless, the enhanced efficiency and digital capabilities of EPIDs make them a valuable tool in contemporary RT.

Historically, radiographic films (port films) were positioned behind the patient to capture images. This approach was laborious due to the time required for film processing and assessment, and it was constrained by a setup accuracy limitation of approximately 5 mm (Barry, et al., 2012). Subsequently, EPIDs affixed to linacs with robotic arms became part of clinical practice. The digital images generated by EPIDs enable online treatment verification and comprehensive analysis. Furthermore, these images are easily accessible and shareable over networks, promoting enhanced data exchange within Radiation Oncology departments.

EPID is grounded on the utilization of indirect detection active-matrix imagers (AMFPIs) and was designed with the purpose of substituting film dosimetry in the realm of treatment field verification. These are commonly integrated as standard apparatus for field verification and quality assurance purposes by vendors of Linacs. The image acquisition process is 2D, exhibiting a 2mm geometric accuracy (Herman, 2005).

2.3. Digitally Reconstructed Radiographs

A DRR image is a 2D representation of an image generated by a 3D medical imaging system that simulates the actions of an X-ray scan (Shen & and Luo, 2008). It is occasionally referred to as a computating virtual radiograph (Serrurier, et al., 2015). Typically, the process of DRR generation is focused on converting volumetric data of a specific body part or the entire human body obtained through a CT scan, from a 3D image to a 2D representation. The process of generating DRR begins with the utilization of an X-ray source that emits radiation into the human body or a phantom, as illustrated in Figure 3. The DRR image is formulated by projecting the intersections of these rays with the 3D volumetric data in the CT volume onto 2D plane and exporting the corresponding 2D pixels by applying a transfer function. A substantial number of rays are necessary to traverse through the CT volume to transfer high-quality 2D pixels and create a usable DRR image (Dorgham, et al., 2009).

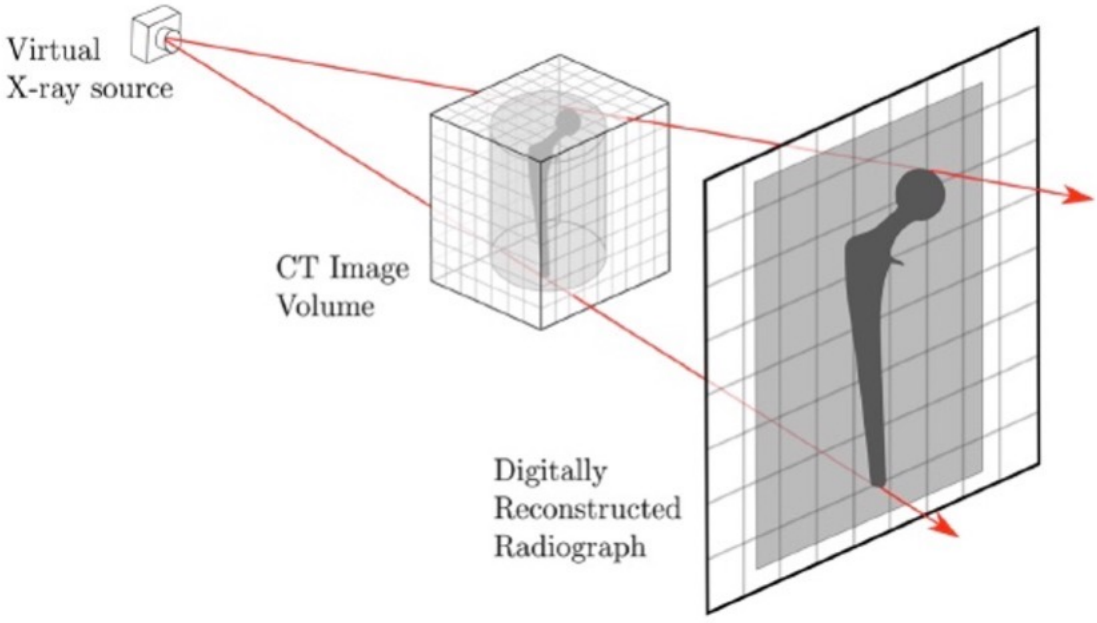

Figure 3: DRRs are produced through the simulations of X-ray propagation within a volumetric CT (Malan, et al., 2016).

Although DRRs are generated after the patient's departure from the CT room, there is utility in acquiring and reviewing CT scout or reformatting CT data before moving the patient. One example is the use of reformatting CT data or CT scout to detect potential movement of the patient during the scan acquisition process. A concise review of these images can help in determining the necessity of repeating the scan while the patient is still positioned on the CT couch. Furthermore, marking field reference or field shapes on the skin of the patient may necessitate the creation of the CT scout or topogram while the patient is still positioned on the CT table (Nagata, et al., 1990; Berlin, 2014).

The primary disadvantages associated with the DRR generation procedure involve the extensive ray-casting operations and computationally heavy mathematical calculations that need to be completed (Dorgham, et al., 2009), which raise the process's overall time complexity. The process of creating a full DRR image is time-consuming due to these drawbacks. As a result, various methodologies have been developed to expedite the DRR generation process. Nonetheless, the majority of the proposed algorithms aimed at enhancing these methodologies so far are capable of delivering the necessary DRR output only at a time complexity rate of $O(N^3)$ (Shen & and Luo, 2008).

2.4. 3D Cone Beam Computed Tomography

A RT delivery error is any discrepancy from the intended or planned treatment. RT practices inherently involve uncertainties, including mechanical uncertainties associated with treatment unit parameters such as treatment table and gantry movement, patient-related uncertainties concerning their ability to remain still on the treatment couch and cooperation during treatment, and geometrical uncertainties involving target motion and positioning. IGRT specifically addresses geometric uncertainties which can be interfractional or intrafractional (Van Herk, 2004; Rasch, et al., 2005). In 2001, CBCT became commercially available for dentomaxillofacial imaging (Mukherji & Miracle, 2009). CBCT has since been identified as a promising tool for RT application, particularly in IGRT because it helps in reducing setup errors before each treatment session. To validate the positioning of the patient, a CBCT system mounted on the linac captures images of the patient while in the treatment position. Any movement of the target region (intrafractional and interfractional movements) during treatment leads to lower dose being delivered to the target. Only by reducing the PTV margins can the

target dose be increased, as this reduces the dose spill to adjacent normal tissues, enabling safer dose escalation and thereby improving TCP (ICRU, 1999; Peng, et al., 2009).

CBCT, whether MV or kV, these systems comprises amorphous silicon detectors; However, only kV CBCT System have retractable X-ray tubes, while MV CBCT uses treatment beam. These detectors are either perpendicular to the radiation beam axis (Elekta Synergy, Varian OBI) or parallel to it (Siemens Artiste). These can perform 2D, CBCT, and fluoroscopic imaging. Another system (Vero, BrainLAB) comprise an O-ring mounted gimbaled X-ray treatment head with two kV X-ray tubes, an EPID, and two flat panel detectors. This O-ring is capable of rotating 360° around the isocenter and can be tilted 60° along its vertical axis. Geometric accuracy is 1 mm or less, and allowing for 2D and 3D alignment with X-ray volumetric images or DRRs derived from planning CT datasets. Scanning is accomplished by rotating the gantry in a continuous partial or full circle around the treatment table. In thoracic and abdominal sites, respiratory motion during acquisition can cause blurring, resulting in images that represent an average organ position. CBCT also allows the monitoring of interfraction setup, as well as anatomical changes due to organ filling (e.g., rectum, bladder) or fluctuation in patient weight. KV CT provides superior contrast resolution than MV CT, but limitation may arise due to scatter from bulky patient anatomy and artifacts from prostheses. The imaging dose from a single CT scan is typically 30-50 mGy, and with daily imaging over the treatment course, the cumulative exposure may reach approximately 500-1500 mGy. While this additional dose is usually acceptable in adult radiotherapy, it highlights the importance of minimizing and optimizing exposure, especially in children and in highly radiosensitive regions (Jaffray, 2007; McBain, et al., 2006; Morin, et al., 2006; Pouliot, et al., 2005; Murphy, et al., 2007).

However, in cone beam geometry, 3D volumetric data can be reconstructed directly from 2D volumetric data, a process known as cone-beam reconstruction. The most widely used approximate reconstruction technique for cone-beam projections acquired along a circular trajectory around a fixed isocenter is the Feldkamp, Davis, and Kress (FDK) algorithm, as shown in Figure 4. The FBP reconstruction is extended by the FDK algorithm. The measured cone-beam in this technique are forward projected using the same ray geometry after being pre-weighted, filtered, and finally back projected (Feldkamp, et al., 1984).

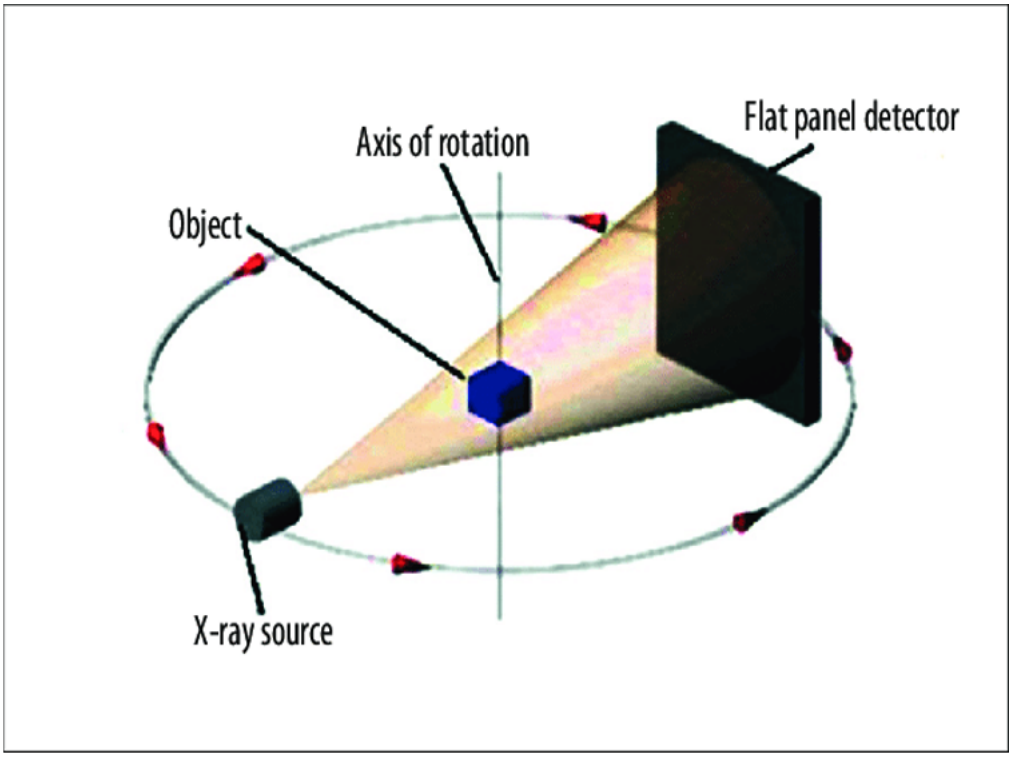

Figure 4: CBCT geometry schematic illustration (Srinivasan, et al., 2014).

The utilization of CBCT to determine the discrepancy between the planned and actual treatment position is an essential component of IGRT (Grills, et al., 2007). This difference is measured as a shift in the treatment field position by comparing CBCT images with their corresponding planning reference CT. Setup errors consists of both random and systematic component and are evaluated along the lateral axis (X), longitudinal axis (Y), and a depth or posterior-anterior (Z) axis, with rotational correction also possible (Van Herk, 2004). IGRT using kV-CBCT can provide precise 3D volumetric data on patient anatomy and target localization at the treatment position, significantly improving RT delivery accuracy. This is accomplished through automatic rigid body image registration algorithms, which register CBCT images with the reference CT images used for treatment planning. However, acquiring CBCT images introduces an additional radiation dose, which is clinically relevant and poses potential risks to the patient. Strategies to mitigate this dose such as protocol optimization (adjusting kVp, mAs, field size and rotation angles) and adaptive imaging frequency, have been proposed. However, this remains an active research area, particularly concerning paediatric safety, long-term risk and integration of new technologies, such as surface-guided radiotherapy (SGRT), to reduce or even replace repeated CBCT scans (Seravalli, et al., 2024; Vassileva, 2025).

2.5. Image registration

Multimodal medical image registration techniques initially surfaced during the 1990s. To provide more detailed patient information and enhance clinical treatment and diagnosis, images acquired from the same patient at different times and with different imaging modalities must be merged and aligned during the clinical treatment process (Sun, 2023). According to the image dimension, medical image registration techniques are classified as 2D-2D registration, 3D-2D registration, and 3D-3D registration. A 3D-2D matching technique aligns the projected image geometrically with the reference image after projecting the 3D object onto the 2D reference image plane. These techniques determine a geometric transformation through optimal registration, ensuring that the 3D object projection closely resembles the 2D reference image in space (Markelj & et al., 2012).

With advancement in IGRT, particularly the introduction of onboard imaging system, patient, patient setup accuracy has significantly improved, leading to a greater confidence in tumour dose coverage. Unlike the early IGRT, which relied on 2D film and patient bony anatomy for positioning verification (Jaffray, et al., 2007; Li, et al., 2011). An internal target may be localized and positioned using either in-room 2D KV imaging or 3D CBCT, with each modality offering distinct advantages for setup verification. While 2D kV imaging provides a high contrast image of implanted fiducials, bony structures, and even soft tissues. Fiducial marker are used in tumour sites with poor visibility on imaging or high motion (prostate, lung, and kidney) to improve setup accuracy and motion management. A gantry-mounted kV system can provide orthogonal on-board 2DkV (OB-2DkV) images and/or perform half or full rotational scans around the linac isocenter to generate CBCT images. Examples of such systems are the Elekta Synergy system (Elekta Inc., Stockholm, Sweden) and Varian On-board imager (Varian Medical System, Palo Alto, California) (Kim, et al., 2011 ; Peng, et al., 2010; Kord, et al., 2021).

2.6. IMRT Technique

IMRT was introduced into clinical practice in the late 1990s (Macchia, et al., 2017) as an advanced technique in RT used for treating both malignant and benign tumours. This technique uses advanced technology to precisely modulate photon radiation beams, enabling them to conform to the shape of the tumour (Bortfeld, 2006). The integration of contemporary imaging modalities, including ultrasound, CT, MRI, PET, and the combined PET/CT, along with the

development of new delivery technique, has greatly improved its effectiveness as a treatment option for cancer patient (Purdy, 2008). IMRT enables the delivery of highly conformal dose distributions, while tight margins arise from robust QA program aimed at minimizing systematic and random errors in the treatment delivery process. These programs include optimized machine QA, imaging procedure, immobilization devices, and clinician review of set-up images, which allow margin reduction without compromising target coverage, but still risk missing microscopic tumour fragments during treatment (Cannon & Lee, 2008; Chen, et al., 2011), thereby increasing the risk of tumour recurrence. Imaging is crucial in RT, as the target can shift, change shape, or change position or volume during treatment, highlighting the importance of IGRT.

2.7. VMAT Treatment Technique

VMAT, introduced in 2007, is an innovative external beam radiotherapy (EBRT) treatment technique that incorporates continuous modulation of multi-leaf collimators (MLCs) (field shaping), in addition to utilizing gantry speed rotation and dose rate to deliver highly conformal dose distributions efficiently within a short time frame, while maintaining reasonable monitor units (MUs) to be delivered (Teoh, et al., 2011; Oliver, et al., 2009). In this context, VMAT emerges as the most recent RT technique that offers various benefits, including decreased treatment delivery duration when compared to conventional static field IMRT. Notably, in VMAT delivery, adjustments in dose rate, field shapes, and gantry rotation speed can occur simultaneously. These supplementary degrees of freedom enhance the capacity for beam intensity modulation in comparison to IMAT (Macchia, et al., 2017), Figure 5 shows the representation the VMAT treatment delivery technique in 3D view.

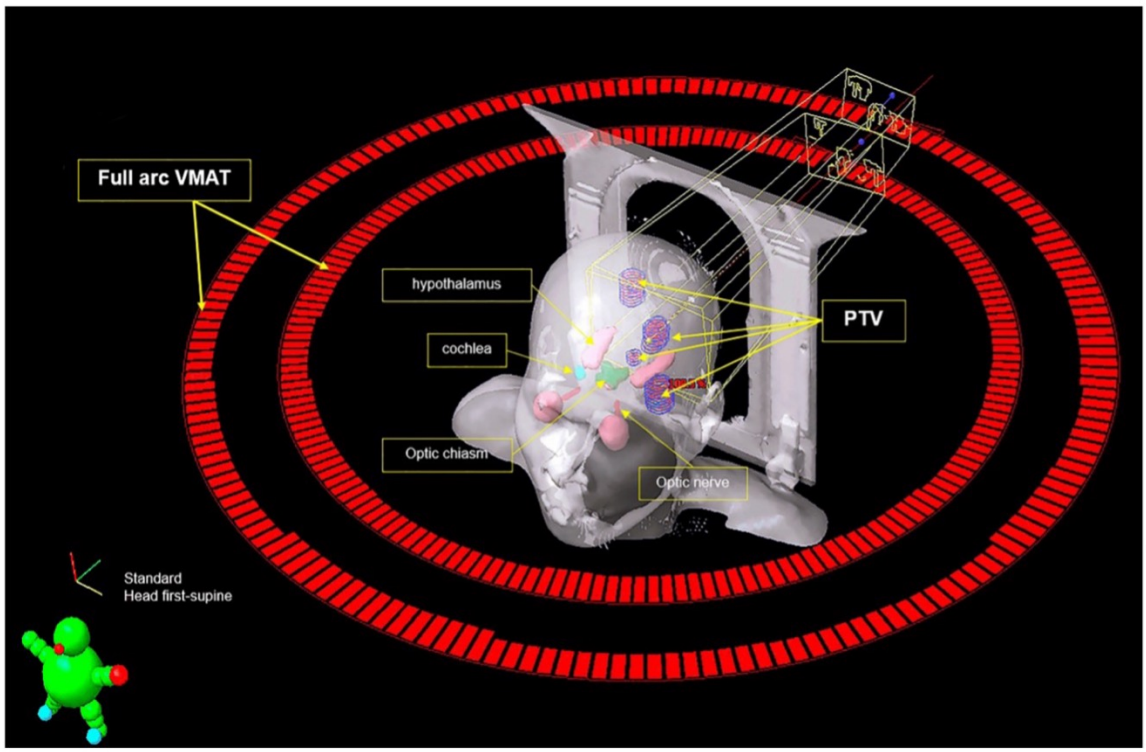

Figure 5: 3D view of VMAT treatment (Yeh, et al., 2023).

Modern RT techniques use modulated beams such as IMRT and VMAT, as well as modulated particle beams such intensity modulated proton therapy (IMPT). The dosimetric advantages of these techniques over 3D-CRT have been extensively studied (Macchia, et al., 2017). Published surveys (Barber, et al., 2017) and comprehensive reviews indicate a transition in clinical practice from 3D-CRT to VMAT (Peng, et al., 2020) specifically, particularly when combined with different dose fractionation schemes such as hypofractionation and Stereotactic Body Radiation Therapy (SBRT). Furthermore, the effects of IGRT and motion management on dose delivery, target positioning accuracy, and reproducibility necessitate a thorough evaluation of the collective clinical impact of these advanced practices with modulated therapies.

2.8. Target Volumes and Organs at risk

RT planning and treatment delivery involve a series of sequential steps during which geometric errors or discrepancies may arise between the planned intended treatment and the treatment delivered. Such discrepancies can occur during target volume delineation, creation of treatment plan, or variations in patient positioning during treatment. To account for these geometric uncertainties a 'safety' margin is added around the tumour volume identified on the CT scan. The delineation of these margins is guided by the guidelines provided by the International Commission on Radiation Units and Measurements (ICRU) reports 50 (ICRU, 1993), 62 (ICRU, 1999) and 83 (ICRU, 2010), which define the volumes utilized for margin creation, as shown in Figure 6.

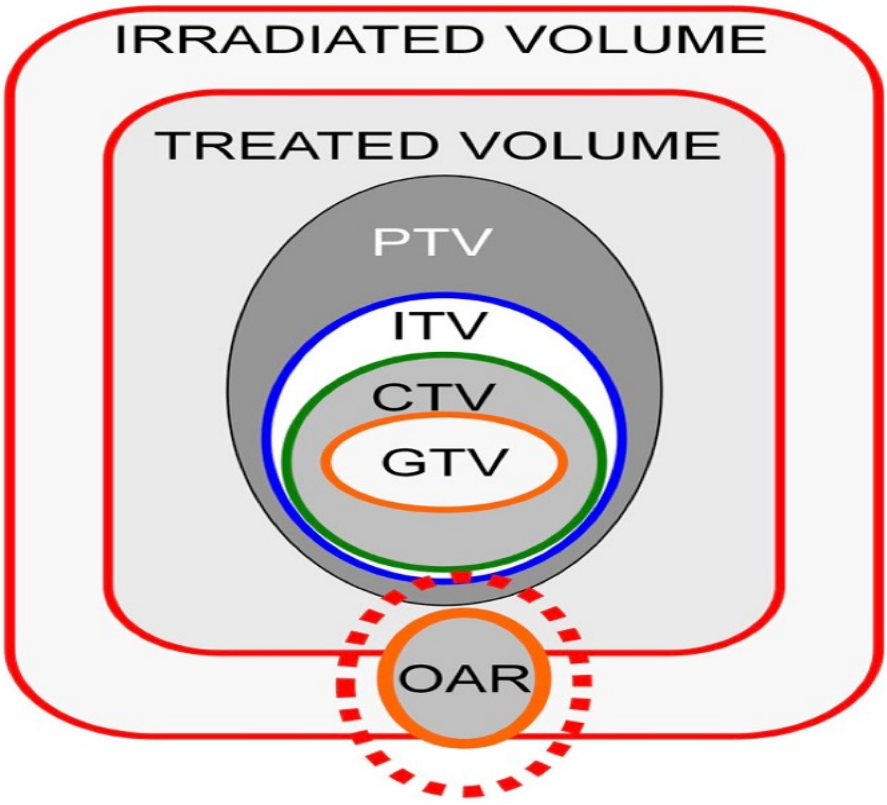

Figure 6: Diagram illustration of ICRU report 50, 62, and 83 volumes (ICRU, 1993; ICRU, 2000; ICRU, 2010).

2.8.1. Gross Tumor Volume (GTV)

The GTV is the gross demonstrable extent and location of the tumour. GTV may comprise a primary tumour, distant metastasis, or metastatic regional nodes (ICRU, 2010). The GTV is

typically based on data acquired from various imaging modalities, including MRI, CT, ultrasound, etc.

2.8.2. Clinical Target Volume

The CTV refers to a specific tissue volume that contains a GTV and subclinical microscopic malignant cells that must be eradicated. adequate treatment of this volume is essential to successfully achieve the therapeutic goals of either cure or palliation (ICRU, 1993).

2.8.3. Internal Target Volume

The delineation of the Internal Target Volume (ITV) comprises the CTV along with an additional margin to accommodate uncertainties related to the CTV's dimensions, geometry, and position within the patient. This margin, known as the internal margin, primarily account for physiological motion such as respiratory, cardiac activity, and bladder or rectal filling. Hence, the ITV is not prevalent in all EBRT treatment plans but is delineated depending on the treatment site. Importantly, the internal margin distinguishes itself from the setup margin. The use of the ITV is particularly relevant in clinical situations where the uncertainties regarding the CTV location are more significant than setup uncertainties, or when these uncertainties are independent. The ITV serves as an optional tool to facilitate the delineation of the PTV (ICRU, 2010).

2.8.4. Planning Target Volume

The PTV represents a geometric principle that has been introduced for the purpose of treatment planning and evaluation. It is designed to ensure that the prescribed dose is delivered to the entire CTV with clinically acceptable certainty, despite geometric uncertainties like organ motion and setup variation. The PTV also incorporates margins to accommodate both internal and setup uncertainties, thus making it essential for absorbed dose prescription and reporting (ICRU, 2010).

2.8.5. Organ at Risk

OAR, also known as critical normal structures, are tissues that can experience a severe damage if exposed to radiation, thereby influencing treatment planning and the dose to be delivered. In principle, any non-target tissue can be considered an OAR. However, those that are classified

as OARs are usually determined based on the location of the clinical target volume or the prescribed radiation dose (ICRU, 2010).

2.9. Setup Errors

Setup errors, although they are undesirable, they are an inherent part of RT. These errors are defined as the discrepancy between the intended or planned and actual position during treatment delivery. The coverage of the target volume depends on the setup margins, which must be carefully optimized to minimize unintended exposure to surrounding healthy tissues. The PTV, which include the CTV with additional margins to compensate for uncertainties in patient positioning, beam geometry and organ motion, is now widely recognized as the standard for RT dose prescription (ICRU, 1994; ICRU, 2000).

2.9.1. Systematic errors

In RT, the term systematic error can refer to errors affecting an individual patient, or an entire treatment population. These errors are consistent, reproducible, and occur in the same direction with similar magnitude. Systematic errors can occur at the beginning of RT or throughout the treatment course. These errors can arise from imaging and simulation such as incorrect patient positioning or laser misalignment, and contouring and planning, including target or OARs delineation errors. They may also result from machine-related issues, like isocenter miscalibration or MLC shift (Morsy, et al., 2019).

2.9.2. Random errors

In contrast, random errors are inherent in any measurement and they occur as different variations in results across repeated measurement. These errors can also occur due to changes in target position, shape, between fractions and during the process of treatment delivery. Additionally, Random errors vary in both direction and magnitude with each treatment fraction (Morsy, et al., 2019). Systematic errors shift the dose distribution relative to the target, while random errors results "blurring" effect of the dose distribution around the target as illustrated in Figure 7.

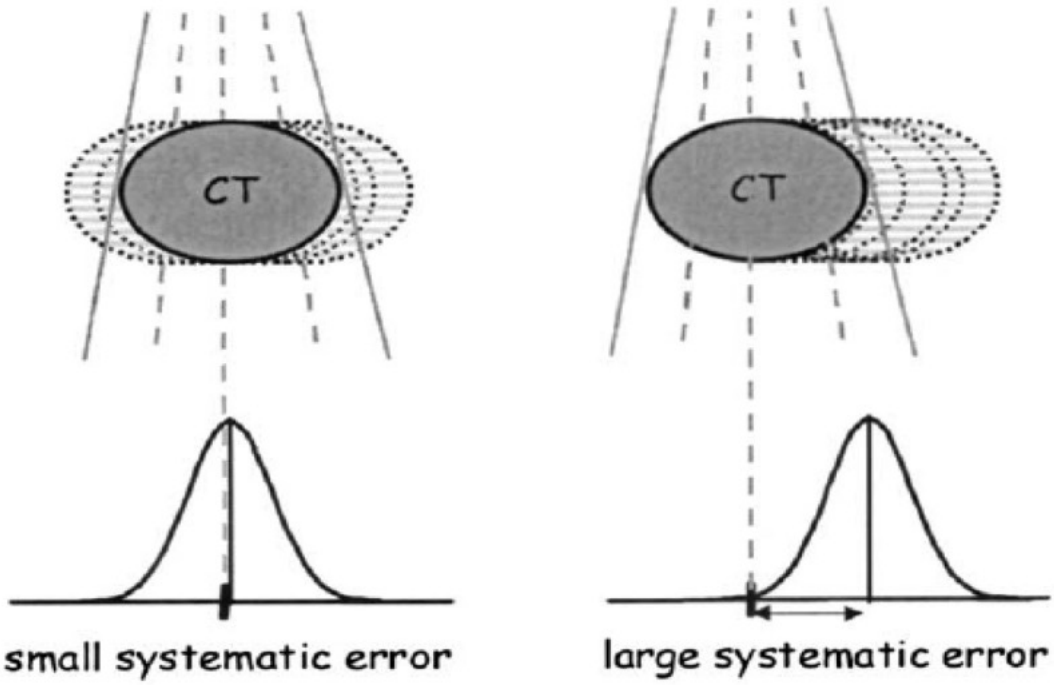

Figure 7: Schematic illustration of systematic errors (Stroom & Heijmen, 2002).

2.10. Literature Review

Several publication have studied the issue of setup errors in RT for nasopharyngeal cancer or head and neck. Li et al. (Li, et al., 2007) analysed 152 patients at seven anatomical sites using a Hi-Art helical tomotherapy system, where daily MV CT images acquired before treatment were fused with planning kV CT images to determine daily setup errors, organ motion, and deformation. Their study reported that setup uncertainties for head and neck vary within 3 mm. Hayder Alabedi (Alabedi, 2023) studied head and neck and breast cancer patients, with head and neck patients immobilized using thermoplastic masks, and all patients were verified using EPIDs. They reported that translational setup errors of 2 mm in the x, y, and z axes, although seemingly small, may affect target coverage and normal tissue sparing. Xu et al. (Xu, et al., 2008) studied 51 patients (19 head and neck, 25 thoracic, and seven abdominal-pelvic) who underwent CBCT scans after initial setup, after repositioning, and following radiation delivery, with images registered to planning CT to quantify setup errors. Their study reported more detailed quantitative data, reporting that translational setup errors in x, y, and z were 1.2 ± 0.9 mm, 1.2 ± 1.1 mm, and 1.0 ± 0.8 mm. These studies highlighted the necessity for accurate patient positioning and, indicating that setup errors vary with tumour location and that even minor setup errors can impact the dose distribution, particularly for highly conformal techniques like IMRT and VMAT. Consequently, the implementation or recommendation of

rigorous quality assurance, image guidance, and patient immobilization devices is important to reduce positional errors and ensuring optimal treatment outcomes.

Chapter 3

3. Materials and Methodology

This chapter provides an overview of the materials and method used to study the dosimetric impact of positional shifts in RT for nasopharyngeal carcinoma. It describes advanced RT tools used to ensure dose delivery accuracy and QA, including the CIRS Shoulder, Head and Neck End-to-End Verification (SHANE) phantom (CIRS Inc., Norfolk, VA, USA), Canon's Aquilion CT system, the Octavius® 4D system (PTW, Freiburg, Germany), and Elekta's Monaco 6.1.2.0 TPS.

This chapter covers the simulation of human anatomy using SHANE phantom, image acquisition using Canon's Aquilion CT system, treatment planning in Elekta Monaco 6.1.2.0 TPS, and accurate dose verification or QA with the Octavius® 4D system. Additionally, it explains the role of the Record and Verify system (RVS) MOSAIQ in transfer and verification of treatment plans, and also the use of Elekta Versa HD linac to introduce positional shifts (translational).

This chapter also details the imaging and treatment processes, QA protocols, and selection of actual patient data to analyse the effects of position errors on dose calculation.

3.1. Materials

In this study, all measurements were conducted at CMJAH. The materials used to evaluate the dosimetric impact of positional shifts in RT for nasopharyngeal cancer include the CIRS SHANE phantom, which mimics human anatomy for comprehensive treatment planning and dose verification. This section explains the use of CT imaging for the acquisition of anatomical data of the SHANE phantom, as well as the role of Elekta Monaco's TPS role in the optimization of treatment plans.

The Octavius® 4D system plays an important role in patient specific quality assurance (PSQA), while the RVS MOSAIQ ensures accurate data transfer and monitoring throughout the treatment process. The Elekta Versa HD Linac delivered radiation doses and enabled the introduction of translational shifts on Octavius® 4D phantom to evaluate their impact on dose distribution and treatment accuracy. Together, these materials form the basis of the study's approach to analysing and reducing position errors in RT.

3.1.1. Anthropomorphic Phantom: CIRS Shane phantom

Anthropomorphic phantoms are important in evaluating image quality and simulating medical procedures. They are also developed for research purposes across different imaging modalities. Phantoms composed of tissue-equivalent materials effectively mimic human anatomy and its attenuation characteristics. This ability enables researchers to calculate absorbed doses to organs, thereby increasing treatment efficacy while protecting normal organs (Ramos, et al., 2017). Anthropomorphic laboratory phantoms are invaluable tools in RT treatment planning, facilitating precise estimation of the dose distribution mapping. This research used the anthropomorphic CIRS Shoulder, Head and SHANE phantom, as illustrated in Figure 8. This phantom mimics typical human anatomy and includes external markers for accurate positioning on the treatment table during both imaging and treatment. In addition, the SHANE phantom consists of four pre-defined ion chamber channels that allow for precise placement of detectors using special chamber cavity rod. This enables the insertion of ionisation chamber for accurate point dose measurement. The CIRS dose verification Head and Shoulder Phantom is explicitly designed for end-to-end testing of the TPS from image acquisition to dosimetry verification.

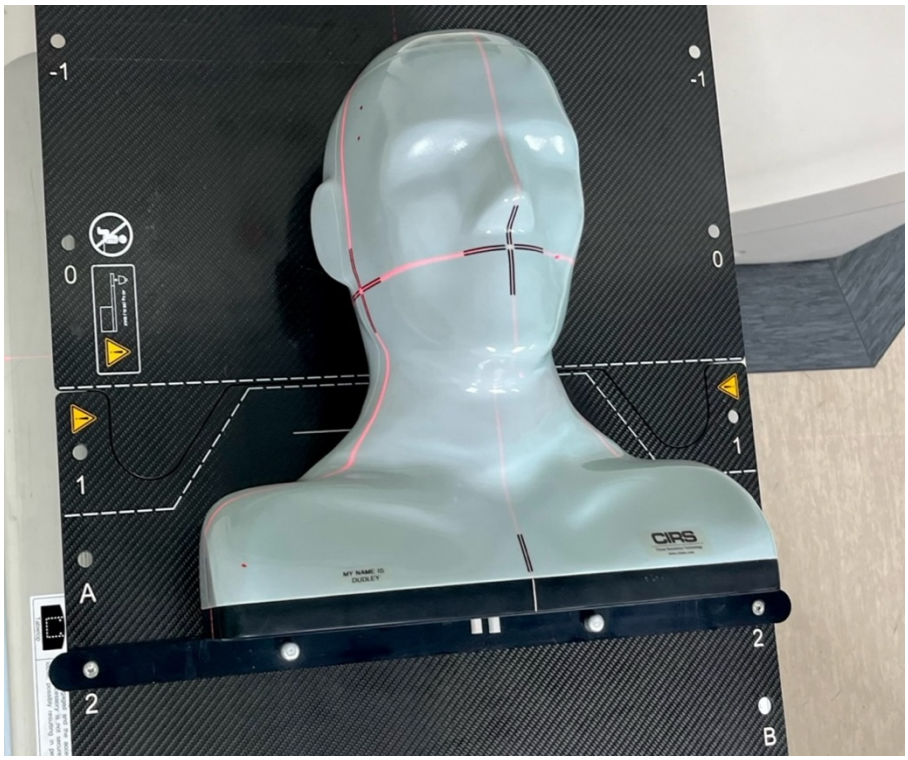

Figure 8: SHANE phantom.

3.1.2. Computed Tomography: The AquilionLB V6.6 system

CT is a medical imaging technique that provides cross-sectional images of a person's body and allows visualisation of organs and tissues, which is helpful in diagnosing various medical conditions, such as cancer, neurological disorders, cancer, and heart disease. CT is a computerised X-ray imaging procedure in which a narrow X-ray beam rotate around the patient generating image projections at various angles that are processed by the machine's computer to create cross-sectional images or slices. After the scanner has gathered these tomography images, they are stacked together using algorithms such as filtered back projection to generate 3D representations of the patient (Rahman, et al., 2023).

This study used a CT scanner to capture detailed anatomical images of the CIRS SHANE phantom, representing human anatomy of the shoulder, head and neck. These images were stacked to create a precise 3D representation of the phantom for RT treatment planning. The CT is crucial for accurately positioning the phantom on the treatment couch, delineating structures such as OARs and target tumours, and providing input to the Elekta Monaco TPS to create a radiation dose distribution. This allowed for proper simulation of treatment and verification of dose delivery. The specific CT scanner used in this study is the fourth-generation Canon AcquilionLB V6.6 CT scanner, as shown in Figure 9.



Figure 9: Canon AcquilionLB V6.6 Computed Tomography.

3.1.3. The Treatment Planning System: Monaco

Elekta's Monaco 6.1.2.0 TPS demonstrates its proficiency in RT treatment planning by creating high-quality treatment plans for various techniques, such as 3D-CRT, IMRT, SRS, and SBRT. This advanced TPS seamlessly combines the accuracy of Monte Carlo (MC)-based dose calculations with robust optimization tools, making it an invaluable asset in radiation oncology (Clements, et al., 2018).

The TPS are integral in RT and significantly contribute to enhancing patient treatment outcomes. Following the import of image datasets and localization of the tumours, the TPS generate a plan for each beam delivery path, detailing how radiation dose is delivered. The as to how the therapy system delivers radiation. Elekta Monaco 6.1.2.0 TPS was employed to create and optimize RT treatment plans for CIRS SHANE phantom. It was specifically utilized for delineating anatomical structures, such as the target tumours (PTV) and OARs. It facilitated the calculation and optimization of dose distribution using advanced algorithms, such as the MC algorithm. Additionally, the TPS was employed in this research to introduce simulated positional errors into the treatment plans of patients undergoing or who had undergone treatment for nasopharyngeal cancer to evaluate their impact on dose distribution and treatment accuracy.

3.1.4. Patient-Specific Quality Assurance System: Octavius® 4D

The Octavius® 4D system (PTW, Freiburg, Germany) comprises a cylindrical, rotating Octavius 4D phantom into which the 2D Octavius 1500 Detector Array is inserted, as shown in Figure 10. An external inclinometer mounted on the gantry continuously monitors the gantry's actual angle and enables the control unit to rotate the phantom accordingly to ensure that the 2D array always remains orthogonal to the beam axis. Hence, this setup enables orthogonal beam output measurement at all angles. The Octavius® 4D system is utilized for dose reconstruction and patient-specific analysis of IMRT QA, with VeriSoft software facilitating the evaluation of IMRT QA plans.

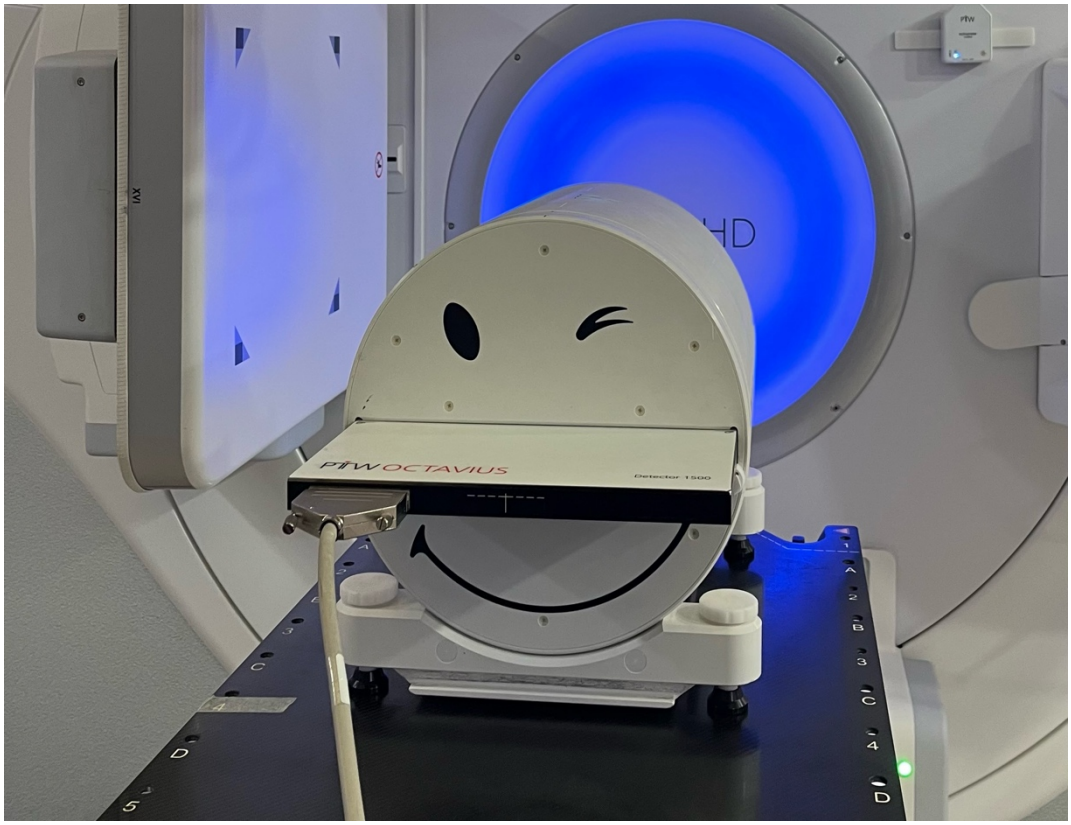

Figure 10: The OCTAVIUS 4D system.

A careful pre-treatment review with a PSQA protocol is a crucial step in RT. This is due to the complexity of the treatment plans and highly sophisticated technology involved in RT. Various tools are available for 2D evaluation, including gafchromic films, EPIDs, arrays of diodes, (such as MapCHECK, SunNuclear corporation), or arrays of ionization chamber, (such as MatriXX, IBA Dosimetry, and 2D-Array Seven29™, PTW) (Urso, et al., 2018).

3.1.5. The Record and verify System: MOSAIQ.

In clinical practice, the implementation a RVS is important, functioning as a fundamental measure to ensure that the prescribed CRT/IMRT is accurately delivered and to guarantee the availability of appropriate reference images within the treatment unit. It is crucial to exercise precise care to avoid any errors during the data transfer process that involves TPS, simulators, and treatment machines (INTERNATIONAL ATOMIC ENERGY AGENCY, 2013). A comprehensive oncology information system, such as MOSAIQ, manages the flow and storage of patient data, including IGRT images, in many RT departments.

The Elekta Versa HD Linac played a key role in this study by delivering radiation doses to the Octavius 4D phantom, simulating real patient treatment conditions. By introducing controlled

translational shifts in the x, y, and z axes, the linac helped assess the impact of the positional errors on dose distribution. MOSAIQ RVS was integral to ensuring the proper transfer and execution of treatment plans created in the Monaco TPS. It managed patient data. And supported PSQA by comparing the administered and planned doses to validate treatment accuracy.

3.2. Methodology

The measurements performed in this study were carried out on the anthropomorphic CIRS SHANE phantom and the Octavius® 4D system to investigate the dosimetric impact of the positional shifts in RT for nasopharyngeal cancer. This study employs advanced imaging, treatment planning, and dosimetric tools to ensure accuracy in RT delivery. Treatment plans were optimized in the Elekta Monaco 6.1.2.0 TPS, and dose calculations were done using the MC algorithm. Additionally, real patient data was utilized further to evaluate the dosimetric impact of the positional errors, ensuring that the study's findings are applicable to actual clinical scenarios.

The CIRS SHANE phantom was positioned by employing the laser positional system on the CT couch to begin the process of image acquisition. A CT scanner was used to acquire anatomical data of the Shane phantom. The VMAT treatment plan that was created using this data in the Monaco TPS then optimised specific dose constraints for tumour volumes and OARs. Positional shifts were introduced to the copied plans to simulate potential errors in patient positioning during treatment. The resulting dose distribution was analysed to evaluate the impact of positional shifts on tumour coverage, OAR, and treatment accuracy. Furthermore, during PSQA, positional shifts were introduced to the treatment couch to assess their dosimetric impact on patients during treatment.

3.2.1. Imaging

The anthropomorphic CIRS Shoulder, Head and Neck phantom was positioned on the CT table using laser alignment markers (crosshairs), and radio-opaque markers were placed on the crosshairs as they were used for a reference point, and the treatment position of the phantom was head first supine as shown in Figure 11, and the phantom underwent CT scan to acquire anatomical data of head and neck, and the reference CT scan was obtained using 3.0 mm CT slice thickness. After the acquisition of CT data, it was transferred to the Elekta Monaco 6.1.2.0

TPS and imported using the CT- electron density (ED) calibration curve. This enabled Image delineation, dose prescription, and plan evaluation, leading to the creation of a VMAT treatment plan for this study.

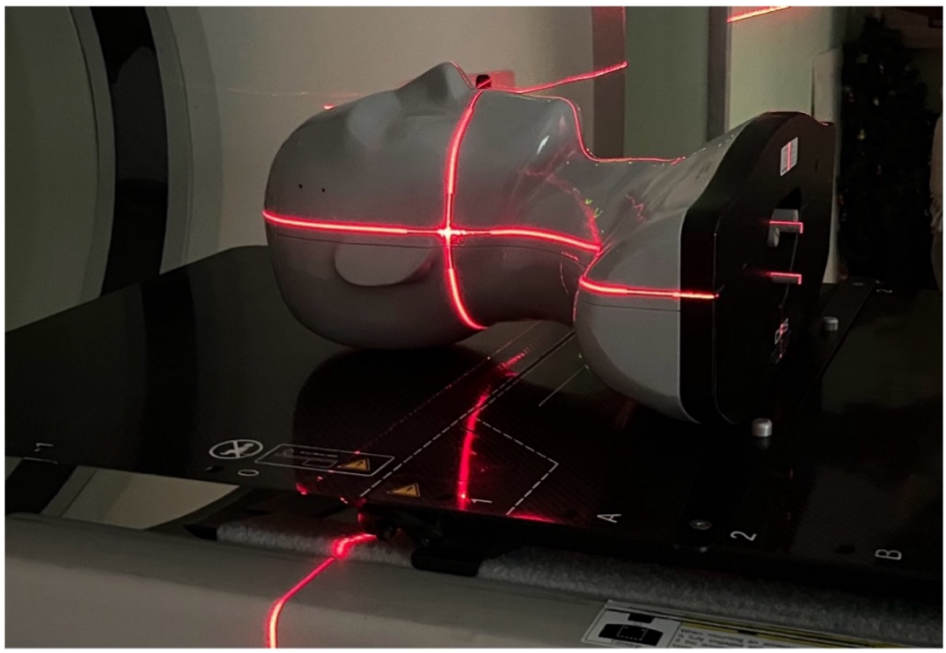

Figure 11: CIRS Shoulder, Head and Neck Shane phantom. The treatment position of the phantom was head first supine on the CT simulation.

3.2.2. Planning

The image delineation process commenced once the CT data was imported into the TPS. This step involved defining and contouring the ICRU volumes (GTV, CTV, ITV, and PTV), including PTV_7000, PTVn1_6000, and PTVn2_5400, which were delineated according to IAEA METHODOLOGY FOR ON-SITE END-TO-END IMRT/VMAT AUDIT (Kazantsev, et al., 2019) as shown in Figure 12, along with delineation of OARs such as spinal cord, parotid glands, and brainstem. Additionally, the dose was prescribed to the PTV, and the selected delivery technique for head and neck case was VMAT. A VMAT plan was created using a pre-defined template in Elekta Monaco 6.1.2.0 TPS. The isocenter was placed at the geometric center of PTV_7000, and two full rotational beams (arcs) were employed to ensure optimal coverage. Cost functions and dose-volume objectives were assigned to both PTVs and OARs in accordance with the IAEA METHODOLOGY FOR ON-SITE END-TO-END IMRT/VMAT AUDIT (Kazantsev, et al., 2019) and QUANTEC guidelines, ensuring adequate tumour target coverage. The plan was then optimized to achieve target coverage while respecting OAR constraints.

To evaluate the impact of setup errors, the optimized VMAT plan was copied to generate multiple VMAT plans, which were modified by systematically shifting the isocenter by 1 mm increments starting from 1 mm to 20 mm. These shifts displaced the isocenter from its reference position in the right (Rt), left (Lt), inferior (Inf), superior (Sup), anterior (Ant), and posterior (Post) directions with respect to the SHANE phantom coordinates from CT simulation. Each copied plan with its own specific coordinates was designated a unique name. For instance, a naming convention such as VMAT4-QA1 was used for easy identification.

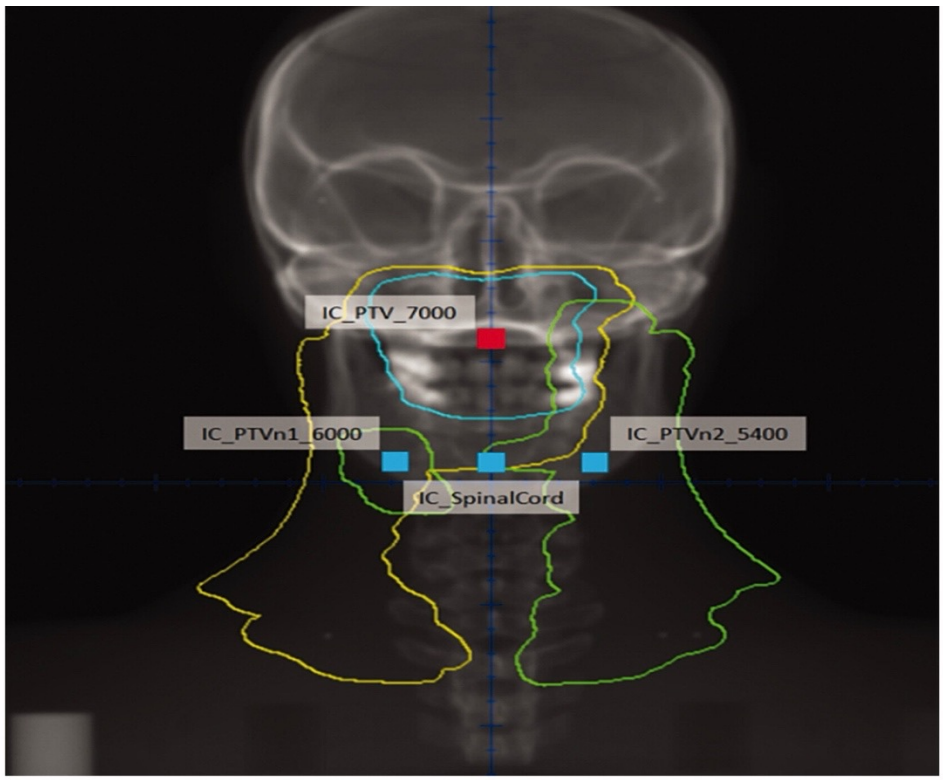

Figure 12: CT scan of the CIRS Shoulder, Head and Neck Shane phantom illustrating the delineated volumes in coronal view (Kazantsev, et al., 2019).

The corresponding plans with applied shifts were recalculated on the TPS without changing any parameter other than the isocenter position, as illustrated in Figure 13. Upon introducing the positional shifts to the QA plans, a DVH was employed for plan evaluation, and a total of 120 shift plans were analysed and compared with their respective reference (original) plans to ensure the appropriate dosimetric impact of the shifts on the tumour coverage and OARs. The investigated plans with shifts were evaluated and recorded. The Original VMAT treatment plan was approved and then sent to MOSAIQ for PSQA and treatment purposes.

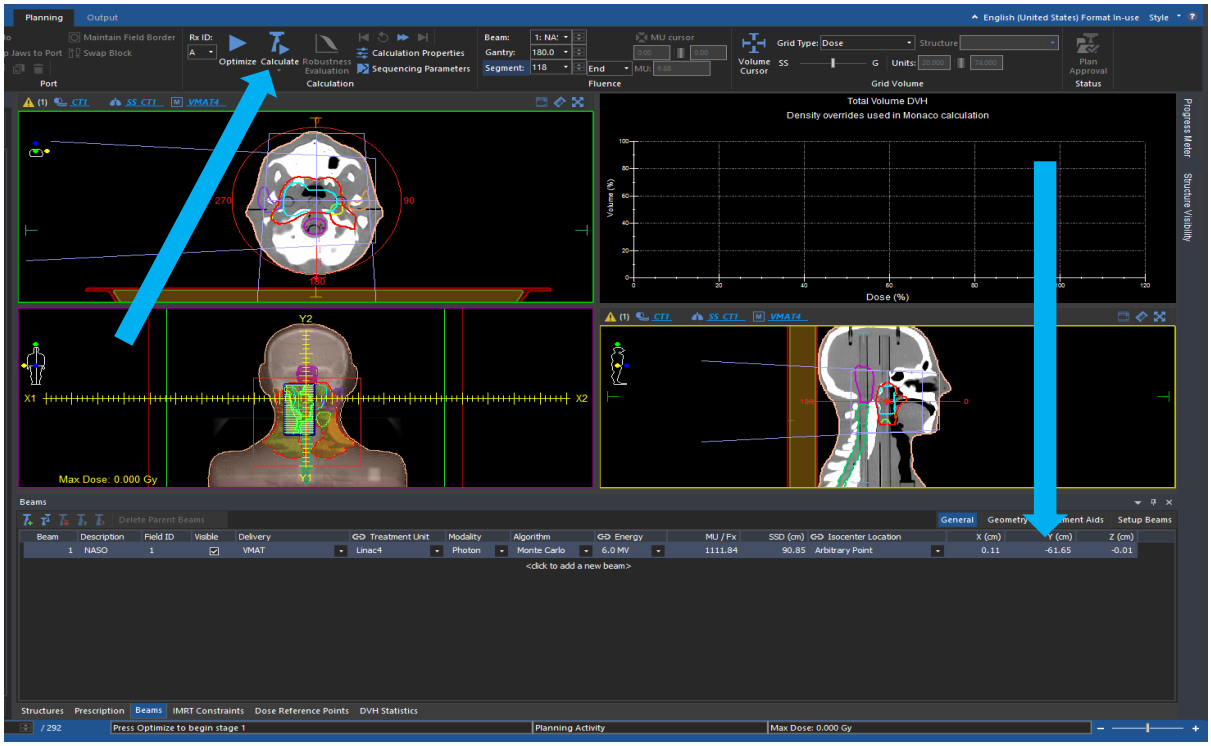

Figure 13: Illustrates the recalculation of the QA plans with shifts on the treatment planning system while varying the isocenter position.

3.2.3. Patient-Specific Quality Assurance

Once the original plan with no shifts was imported into the MOSAIQ RVS, the corresponding QA plan was exported from the TPS to the PSQA system. The OCTAVIUS 4D phantom, which mimics the patient geometry, was positioned at the machine's isocenter according to the planned treatment setup, ensuring alignment with the machine's isocenter, as shown in Figure 14.

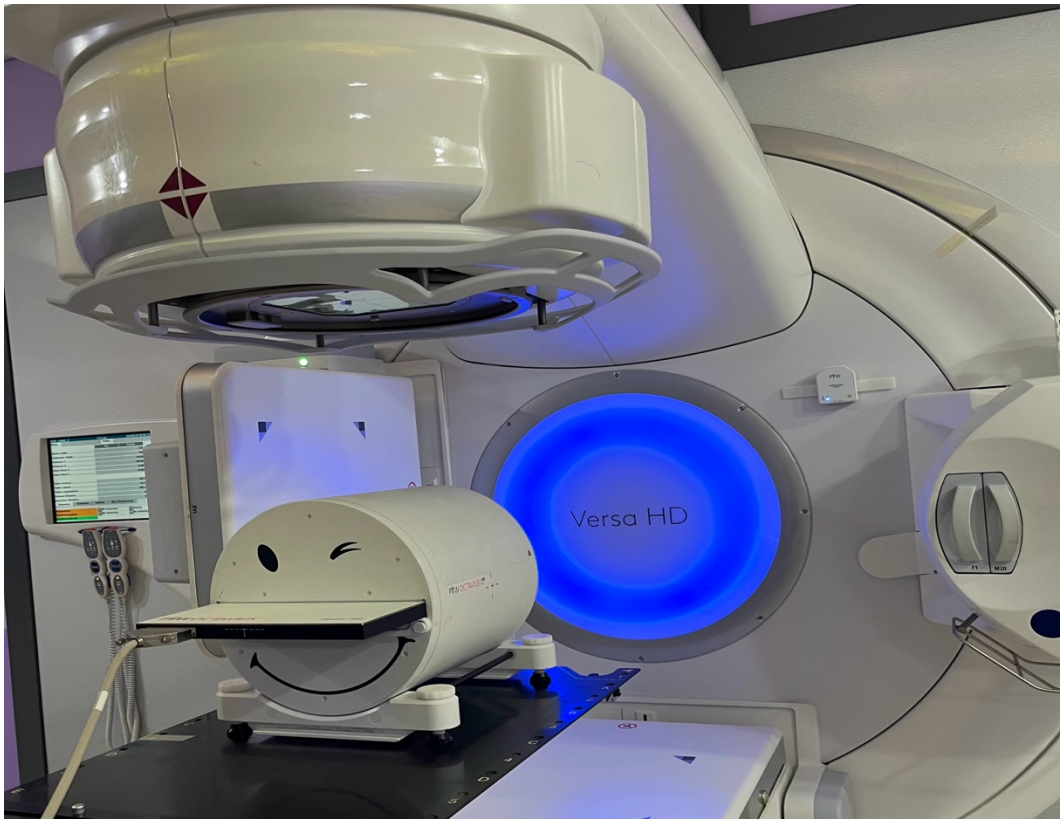

Figure 14: The 4D phantom in isocentric position on the treatment table.

Translational shifts in the x, y, and z directions were manually introduced by moving the couch using the control console, as shown in Figure 15. These shifts ranged from -20 mm to 20 mm, with 1mm increments (from ±1 mm to ±5 mm) and then 5 mm increments (from ±5 mm to ±20 mm). The introduced shifts were recorded and evaluated, and the measured dose distribution resulting from these translational shifts was compared with the planned dose distribution from TPS using VeriSoft software.



Figure 15: Illustration of how positional shifts were introduced through couch movement in lateral, longitudinal, and vertical directions.

3.2.4. Patient selection

Following the ethics approval, this retrospective study consisted of 8 selected patients who underwent a nasopharynx cancer treatment from 2020 to 2023 with a dose prescription of 66.0 Gy distributed in 30 fractions, giving 2.0 Gy per fraction. The treatment modality employed was VMAT with at least two full rotation beams (arcs). An example from one of the patients illustrating the two rotational beams (arc) of a VMAT plan is presented in Figure 16. The study focused on patients who were referred to the hospital for RT and who successfully underwent their treatment, with corresponding records stored within the local radiation oncology department database. The Wits Research Ethics Committee of the Faculty of Health Sciences approved the request to access the patient data at CMJAH.

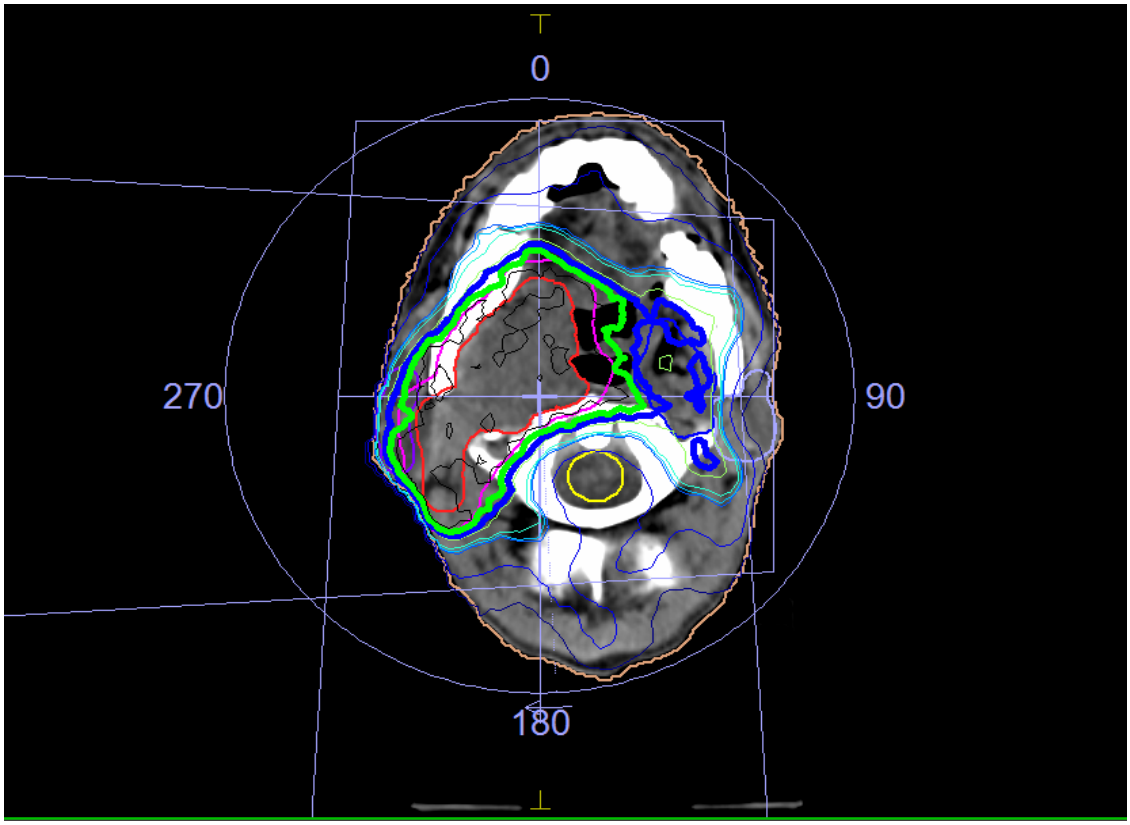

Figure 16: Transverse view of VMAT plan with at least two full rotation beams (arcs).

3.2.5. Positional Shifts and Dose calculation

The randomly selected eight patients who underwent treatment plans for nasopharynx cancer had their original approved plans copied, and then translational shifts were introduced for these same plans. Each copied plan with its specific shift coordinates was given a unique name, such as SINONASALB1, for easy identification. Positional shifts of the beam were introduced to these copied plans in various directions: lateral (x), longitudinal (y) and vertical (z), as illustrated in Figure 17. These shifts ranged from 1 mm to 20 mm, with increments of 1 mm (from 1 mm to 8 mm) and 2 mm increments (from 8 mm to 20 mm). The plans with shifts were recalculated but not optimised upon introducing the shifts, as shown in Figure 17. Optimising the plans would have caused the planning system to try and conform to the PTV despite the introduced shifts, which would have obscured the effect of positional shifts on the dosimetry of the OARs and target coverage.

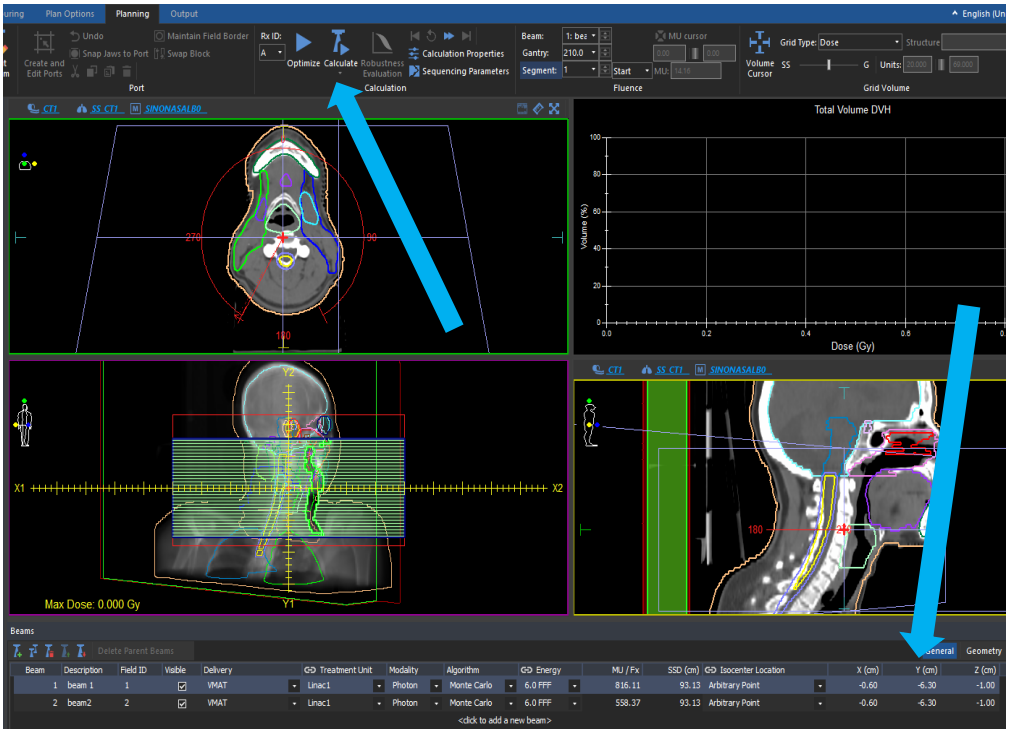

Figure 17: Illustrates how the positional shifts of the beam were introduced on the copied plans and how they were recalculated.

The original treatment plans for all patients were already optimized with the following criteria in Table 1 below to ensure that the dose constraints for OAR according to QUANTEC (Marks, et al., 2010) were met, and the hot spot was defined as PTV receiving 105% - 110% of the prescribed dose. For each of the 8 cases of nasopharynx cancer, 14 shifts were applied to the treatment plans, shifting the isocenter from its reference position in the lateral, longitudinal, and vertical directions with respect to the patient's coordinates. The shift plans were recalculated in the TPS without changing any other parameter than the isocenter position. 672 plans with applied shifts were analyzed and compared with their respective reference plans. These shift plans were specifically generated and recorded for specific setup shifts and not for the entire course of treatment.

Table 1: Dose constraints for Nasopharynx cancer

Structures	Dose constraints
PTV	$D_{95} > 62.7$ Gy
Right/Left Parotid Gland	$D_{mean} < 26$ Gy
Right/Left Cochlear	$D_{mean} < 45$ Gy
Spinal Cord	$D_{max} < 45$ Gy
Brainstem	$D_{max} < 54$ Gy
Brain	$D_{max} < 60$ Gy
Right/Left Lens	$D_{max} < 8$ Gy
Right/Left Eye	$D_{max} < 45$ Gy

Chapter 4

4. Results analysis and Discussion

This study's primary focus is on translational shifts for nasopharynx patients that simulate setup errors in the clinic. The range of shifts was from zero to an exaggerated value of 20 mm. Rotational shifts were excluded from this work. The investigation begins with plans that have been approved and meet dosimetric criteria for both the target volume and the OARs. Translational shifts are then introduced to evaluate the dosimetric consequences. The results map out the dosimetric consequences for the PTV and the OARs calculated by the TPS.

4.1. Translational shifts on a SHANE phantom plan

DVH dosimetric parameters for the PTVs (reference dose) and OAR (mean dose) of the newly generated plans with shifts were obtained for Shane phantom according to the IAEA METHODOLOGY FOR ON-SITE END-TO-END IMRT/VMAT AUDIT (Kazantsev, et al., 2019). The target coverage for PTV_7000 ($D_{98\%} > 66.5$ Gy), PTVn1_6000 ($D_{98\%} > 54$ Gy), and PTVn2_5400 ($D_{98\%} > 48.6$ Gy), which is defined as 95% of the prescribed dose covering 98% of the PTV_7000 and defined as 90% of the prescribed dose covering 98% of PTVn1_6000 and PTVn2_5400, was clinically acceptable for the VMAT plan without any introduced shifts, but the dosimetric parameters changed with the introduction of the positional shifts, illustrating their impact. It is worth noting that the results derived from this phantom study cannot be taken as general tolerances; the same study conducted for a patient population will give more realistic results that can be adopted in the clinic (see section 4.2).

4.1.1. PTV Evaluation

Figure 18 illustrates dose volume coverage for three PTVs, PTV_7000 ($D_{98\%} > 66.5$ Gy), PTVn1_6000 ($D_{98\%} > 54$ Gy), and PTVn2_5400 (($D_{98\%} > 48.6$ Gy), plotted against the translational shifts (in mm), lateral, longitudinal, and vertical.

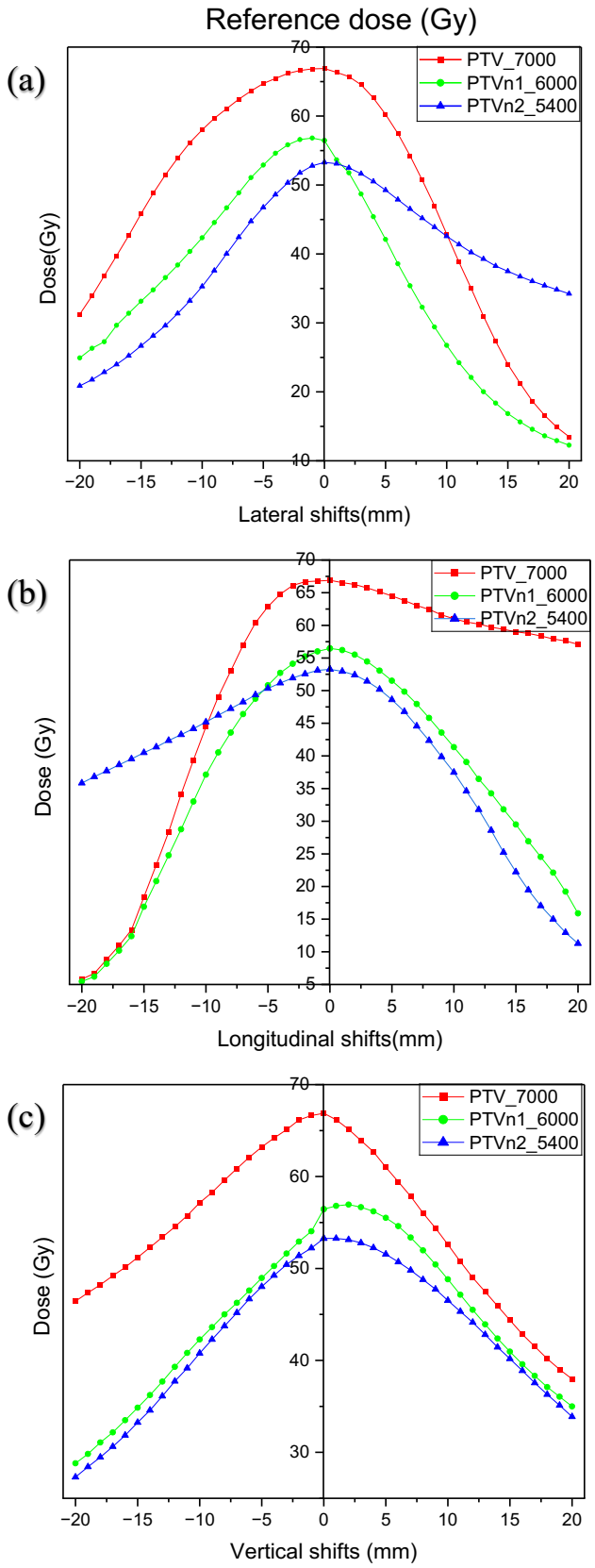

Figure 18: Three PTVs; PTV_7000 (red), PTVn1_6000 (green), and PTVn2_5400 (blue), plotted against the translational shifts; (a) lateral, (b) longitudinal, and (c) vertical along x-axis.

The dosimetric impact of positional shifts varies with dose levels, as shown in Figure 18, with PTV_7000 being the most sensitive to the shifts because of its steep gradient, making accurate or precise patient setup very important in these cases. The dose coverage criterion of PTV_7000 ($D_{98\%} > 66.5$ Gy) fails, and the coverage decreases significantly with lateral shifts beyond -2 mm and +1 mm, as well as longitudinal shifts exceeding -2 mm and +1 mm; however, there is a strong decrease in dose coverage in the inferior direction and vertical shifts beyond ±1 mm. On the other hand, PTVn1_6000 ($D_{98\%} > 54$ Gy) show a more gradual decrease in dose coverage, with lateral shifts impacting dose coverage beyond -4 mm and +1 mm, longitudinal shifts maintaining tolerance up to ±3 mm, and vertical shifts causing dose coverage degradation beyond -1 mm and +6 mm. PTVn2_5400 ($D_{98\%} > 48.6$ Gy) shows the greatest robustness, with the dose coverage criterion failing beyond lateral shifts of -4 mm and +5 mm, longitudinal shifts of -6 mm and +5 mm, and vertical shifts of -4 mm and +8 mm.

Lateral and vertical shifts cause minimal asymmetry in dose reduction across all the PTVs, but longitudinal shifts show more relaxed trends towards the superior direction, especially in PTV_7000, as a result of beam configuration. Vertical shifts show larger shift tolerance, meaning the dose coverage is still within the acceptable limits or above the criterion even with larger shifts because of phantom geometry or central beam alignment. These trends result from asymmetries in beam weighting and dose distribution as a result of phantom geometry or treatment planning parameters, with lower-dose volumes showing a broader dose gradient and sensitivity reduction to these shifts. Overall, the sensitivity hierarchy follows PTV_7000 > PTVn1_6000 > PTVn2_5400.

Clinically, these analyses emphasize the need for accurate or precise patient setup, as even minor shifts result in underdosing in high-dose PTVs or dose spillover, increasing the risk of toxicity to surrounding organs. Implementing real-time imaging and more frequent (maybe daily) IGRT is crucial to minimizing risks, accounting for setup errors, and ensuring accurate dose delivery. Table 2 shows the established positional shift tolerances of the Shane phantom.

Table 2: The established shift tolerance of the PTVs for Shane phantom.

Shift Direction		**PTV_7000 (70 Gy)**	**PTVn2_6000 (60 Gy)**	**PTVn1_5400 (54 Gy)**
Lateral	Right (-)	2 mm	4 mm	4 mm
	Left (+)	1 mm	1 mm	5 mm
Longitudinal	Inferior (-)	2 mm	3 mm	6 mm
	Superior (+)	1 mm	3 mm	5 mm
Vertical	Anterior (-)	1 mm	1 mm	4 mm
	Posterior (+)	1 mm	6 mm	8 mm

4.1.2. OARs Evaluation

Figure 19 presents the mean dose delivered to OARs plotted against the simulated translational shifts. With varying sensitivity, lateral shifts greatly impact dose distribution to both parotid glands, the spinal cord, and the brainstem. The parotid glands are highly sensitive to shifts, with doses exceeding the criterion ($D_{mean} < 26$ Gy) threshold even with minor shifts. The right parotid gland dose increases for negative shifts and decreases for positive shifts, while the opposite occurs for the left parotid gland. At ±20 mm, the mean dose of the right parotid gland increases to approximately 67 Gy, which exceeds the 26 Gy constraint. Longitudinal shifts show less pronounced increases to both parotid glands, but at ±20 mm, the dose to both parotid glands is approximately 34-39 Gy, which also exceeds the constraint. Vertical shows a similar trend to longitudinal shifts, with both parotid glands experiencing a dose increase that exceeds the 26 Gy constraint to approximately 50 Gy at maximum shifts.

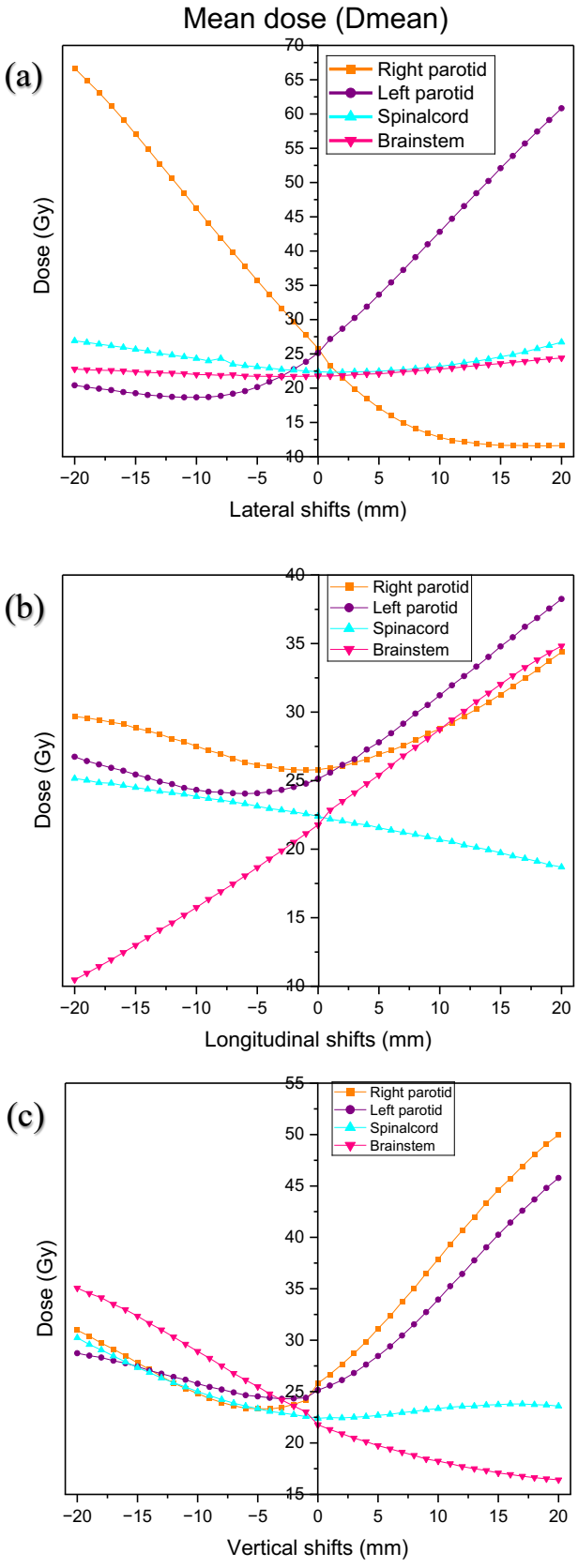

Figure 19: Mean dose of all critical organs plotted again the translational shifts; (a) lateral shifts, (b) longitudinal shifts, and (c) vertical shifts.

The spinal cord dose remains stable across all shifts, with doses consistently below the constraint ($D_{mean} < 45$ Gy). Lateral shifts result in a slight dose increase in both directions, as shown in Figure 19. Longitudinal shifts result in a slight dose increase in the inferior direction and the opposite in the superior direction. Vertical shifts result in less impact, keeping the mean dose below 45 Gy constraint even at ±20 mm. The brainstem is sensitive to these shifts, especially to longitudinal shifts and vertical shifts, but the doses remain below the constraints ($D_{mean} < 50$ Gy) even at ±20 mm. Lateral shifts result in a steady dose increase and remain below the 50 Gy constraint at ±20 mm.

The dosimetric impact varies for all OARs due to their anatomical positioning in relation to the tumour. The parotid glands are most sensitive because of their proximity to the high-dose volumes followed by the brainstem, while the spinal cord remains the least affected by the shifts. The parotid glands are very sensitive, with dose constraint violation occurring even at minor shifts, while the brainstem is sensitive but does not exceed the constraint even at maximum shifts. Only the spinal cord shows relaxed trends with minimal dose variation, as they are the least affected. The results emphasize the need for accurate or precise patient positioning and real time imaging to mitigate the risks of exceeding the constraint of parotid glands, which could result in xerostomia, and that of the brainstem, which could result in necrosis or neurological damage. Table 3 shows the dose constraints threshold for parotid glands, brainstem, and spinal cord.

Table 3: The established shift tolerances of both parotid glands, spinal cord, and brainstem across all directions for Shane phantom.

Shift direction	**OAR**	**Dose constraint**	**Shift range (mm) Violation constraint**
Lateral	Right parotid gland	D_{mean} < 26 Gy	-1 mm and no violation in the left lateral
	Left parotid gland	D_{mean} < 26 Gy	+1 mm and no violation in the right lateral
	Spinal cord	D_{mean} < 45 Gy	No violation
	Brainstem	D_{mean} < 50 Gy	No violation
Longitudinal	Right parotid gland	D_{mean} < 26 Gy	-4 mm and +2 mm
	Left parotid gland	D_{mean} < 26 Gy	-18 mm and +2 mm
	Spinal cord	D_{mean} < 45 Gy	No violation
	Brainstem	D_{mean} < 50 Gy	No violation
Vertical	Right parotid gland	D_{mean} < 26 Gy	-13 mm and +1 mm
	Left parotid gland	D_{mean} < 26 Gy	-11 mm and +2 mm
	Spinal cord	D_{mean} < 45 Gy	No violation
	Brainstem	D_{mean} < 50 Gy	No violation

4.2. Patient Data Shifts: Dosimetric Impact on PTV

4.2.1. Lateral shifts (Left and Right)

In the lateral shifts, the dose distribution shows a symmetric decline, peaking at approximately 65 Gy at 0 mm and dropping below the $D_{98\%} > 62.7$ Gy criterion beyond ±2 mm, as shown in Figure 20. Lateral shifts exceeding ±2 mm result in PTV underdosing of the patients, establishing a 2 mm shift tolerance consistent with acceptable setup error threshold according to Hayder Alabedi (Alabedi, 2023). This sensitivity to the shifts is likely because of VMAT beam configuration, which optimized dose delivery around PTV and suggested that lateral shifts move the target away from high-dose regions. Error bars indicate that at 0 mm, there is minimal variability, but the inter-patient difference increases at ±20 mm.

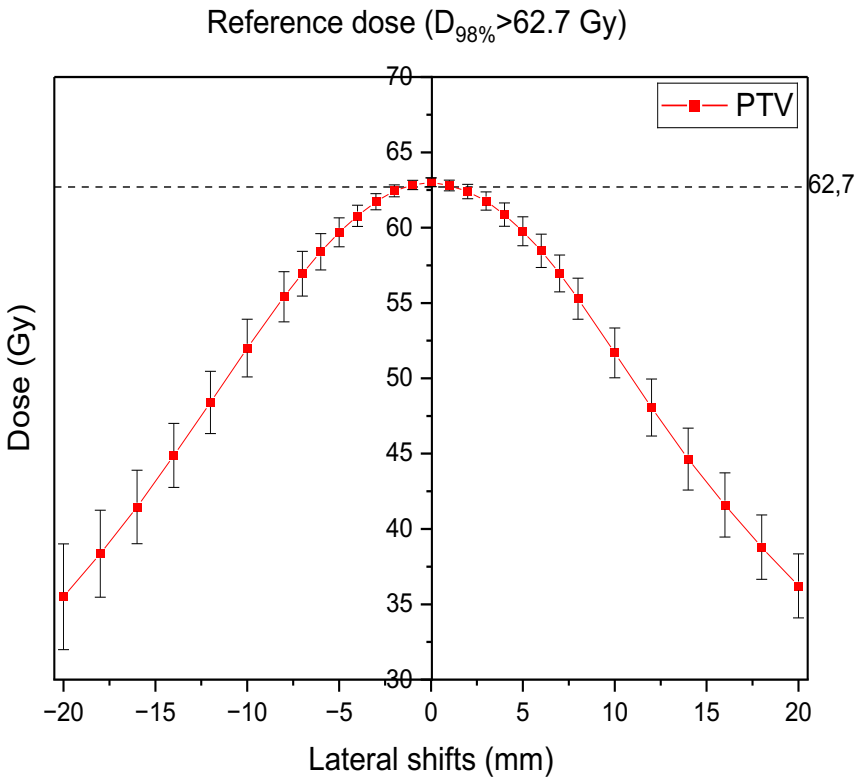

Figure 20: Dose response of PTV to lateral shifts in VMAT radiotherapy plan.

Lateral shifts beyond 2 mm in both directions compromise PTV coverage, increasing the risk of irradiating surrounding healthy organs, which could severely compromise treatment effectiveness, especially in high dose volumes critical for tumour control. Maintaining setup errors within 2 mm is crucial to ensure adequate tumour coverage.

4.2.2. Longitudinal shifts (Superior and Inferior)

In longitudinal shifts, dose coverage decreases, and the $D_{98\%} > 62.7$ Gy criterion fails beyond -2 mm and +3 mm. The established shift tolerances are still consistent with the acceptable setup errors threshold, according to Hayder Alabedi (Alabedi, 2023), but only in the inferior direction. The sensitivity of dose coverage to inferior shifts is pronounced, showing a steep decrease in dose of approximately 70% at -20 mm, as shown in Figure 21. Larger inferior shifts beyond -2 mm should be avoided as they severely compromise the treatment accuracy.

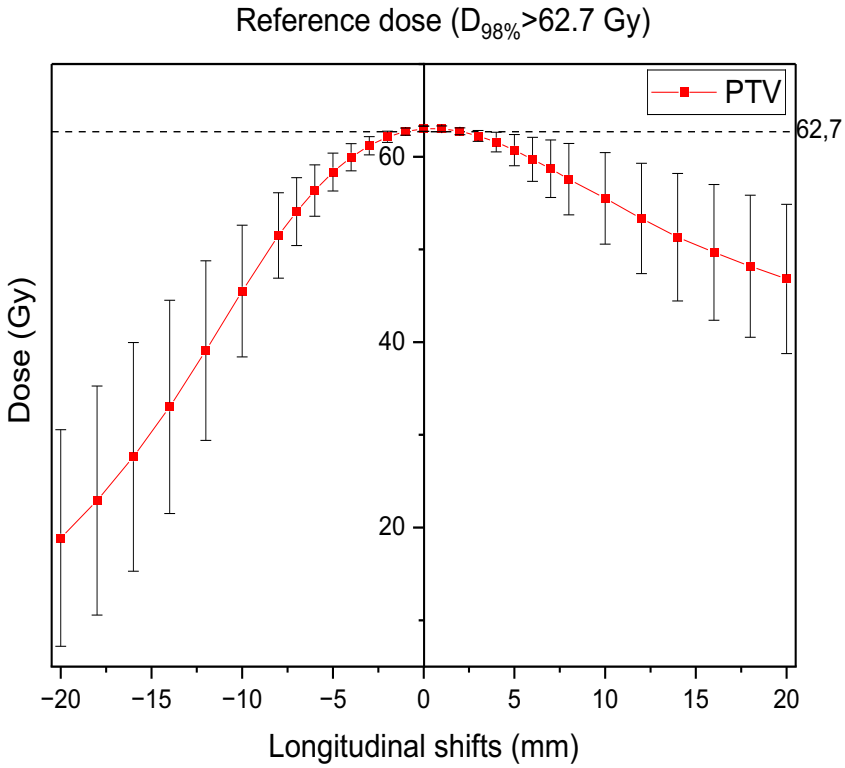

Figure 21: Dose response of PTV to vertical shifts in VMAT radiotherapy plan.

4.2.3. Vertical shifts (Posterior and Anterior)

For posterior shifts, PTV dose coverage also decreases, showing a symmetric decline similar to lateral shifts, resulting in an approximately 40% reduction in dose coverage, as shown in Figure 22. The dose drops below the $D_{98\%} > 62.7$ Gy criterion at ±2 mm, establishing a 2 mm. This shift threshold aligns with that of lateral shifts, and both are consistent with the acceptable setup error threshold, according to Hayder Alabedi (Alabedi, 2023). This symmetrical decrease in dose indicates a uniform beam distribution along the vertical plane, causing a similar dose degradation for both anterior and posterior shifts.

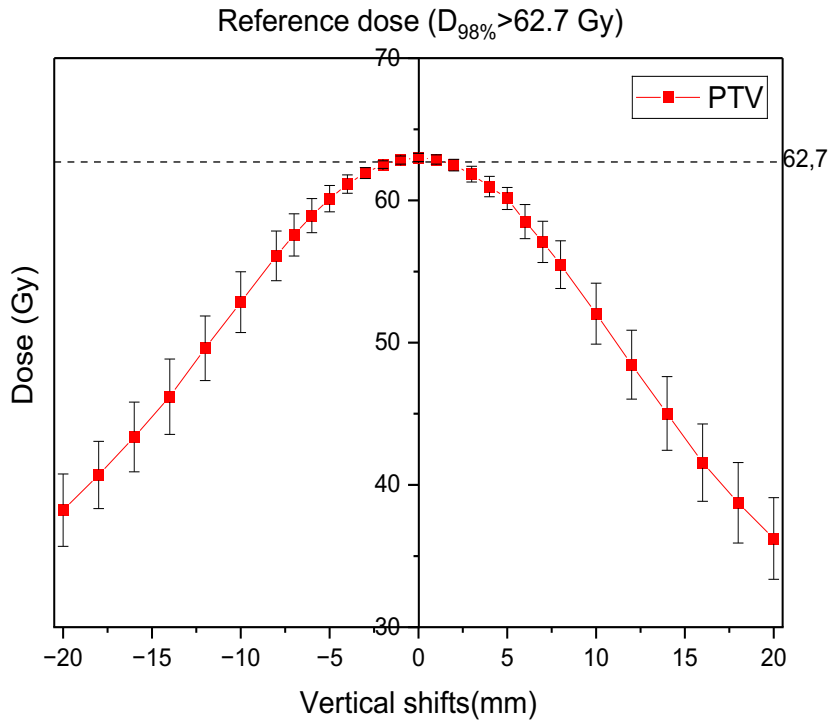

Figure 22: Dose response of PTV to vertical shifts in VMAT radiotherapy plan.

Vertical shifts beyond ±2 mm compromise the dose coverage, increasing the risk of tumour underdosing and reducing treatment efficacy. Vertical shifts impact the PTV dose coverage more at maximum (20 mm) shifts than lateral and longitudinal shifts. This comparison shows that vertical shifts impact decreasing the PTV dose more than lateral and longitudinal shifts. To minimize the risks of overdosing the surrounding healthy organs and underdosing the tumour, accurate patient positioning with enhanced immobilization technique or devices and daily IGRT (e.g., CBCT) is crucial in maintaining adequate dose coverage and ensuring consistent treatment delivery. Table 4 below shows the established shift tolerances of the translational shifts.

Table 4: Established shift tolerances obtained from the calculations based on PTV tolerances

Translational shifts					
Lateral		Longitudinal		Vertical	
Rt lateral	Lt lateral	Inferior	Superior	Anterior	Posterior
2 mm	2 mm	2 mm	3 mm	2 mm	2 mm

4.2.4. Hot spots

Figure 23 below show that positional shifts also negatively impact the hot spots, measured by D2%, which must be less than 105%-110% of the prescribed dose. The graph below illustrate that lateral, longitudinal, and vertical shifts increase the hot spots, and it also indicates that right lateral and inferior positional shifts result in more hot spots. Anterior shifts have less impact as more shifts are introduced. This emphasizes the need for accurate patient positioning in radiotherapy, especially with these translational shifts, to avoid the risks of overdosing the adjacent OARs and underdosing the treated volume.

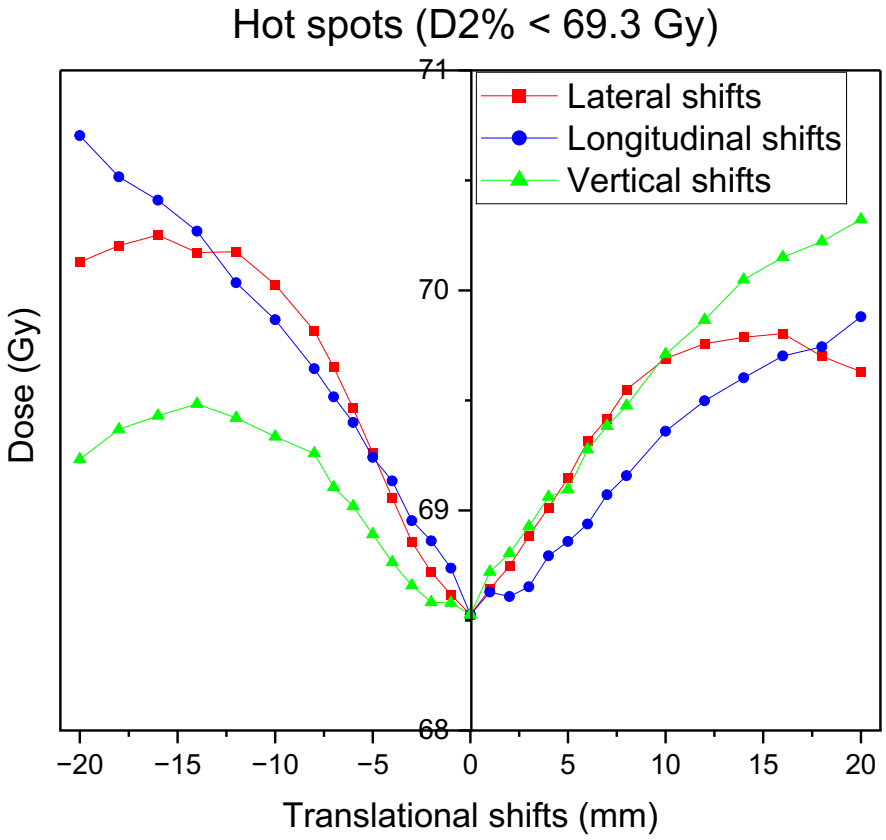

Figure 23: Hotspots (D2%<69.3 Gy) for translational shifts; Lateral, longitudinal, and vertical.

4.3. Patient Data Shifts: Dosimetric Impact on OAR

4.3.1. Lateral shifts

Lateral shifts impact the mean dose to the cochlear, with the left cochlear exceeding its dose constraint at +1 mm and the right cochlear at -14 mm. The right cochlear dose increases for right lateral shifts and decreases for left lateral shifts, while the opposite occurs for the left cochlear, as illustrated in Figure 24. At -20 mm, the right cochlear dose increases to approximately 48 Gy, and at +20 mm, the left cochlear dose increases to approximately 56 Gy, both exceeding the $D_{mean} < 45$ Gy constraint. These excessive doses at maximum shifts of ±20 mm pose the risk of overdosing the critical organ, which could result in ototoxicity and hearing loss.

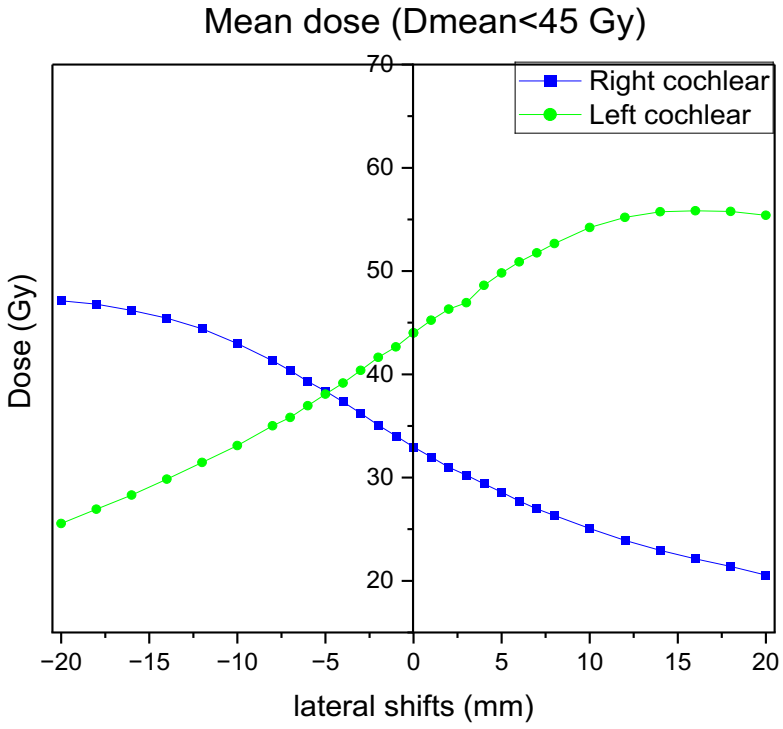

Figure 24: Impact of lateral shifts on mean dose of surrounding critical cochlear organs.

The parotid glands are highly sensitive to the shifts, with their dose constraints failing from the original plan, at 0 mm already above the $D_{mean} < 26$ Gy constraint, as shown in Figure 25. The right parotid gland experiences a dose increase with right lateral shifts and a decrease in dose with left lateral shifts, whereas the opposite occurs for the left parotid gland. At ±20 mm, the dose for both increases to approximately 57 Gy, far exceeding the clinical 26 Gy constraints.

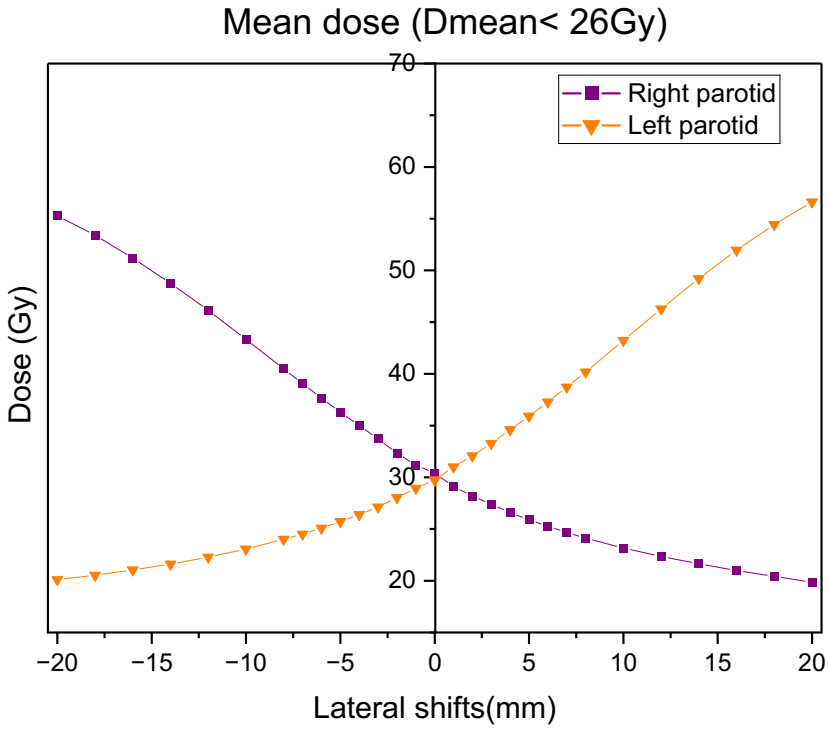

Figure 25: Impact of lateral shifts on mean dose of surrounding critical parotid glands.

Figures 26-27 illustrate the effects of lateral shifts on the dose distribution to the spinal cord, brainstem, brain, lenses and eyes. For eyes and lenses, the left lens exceeds the 8 Gy constraint at +10 mm, while the right lens dose exceeds the 8 Gy constraint at 0 mm and continues to increase with right lateral shifts but decreases with left lateral shift. Both eyes remain below the 45 Gy constraint in both lateral directions. The spinal cord is sensitive to lateral shifts, with the dose increasing in both directions: At +5 mm and -3 mm, the dose exceeds $D_{max} < 45$ Gy constraint. The brain exhibit higher sensitive than the spinal cord and brainstem, with the dose exceeding 60 Gy constraint at 0 mm. The brainstem also shows sensitivity, with the dose exceeding the 54 Gy constraint at -1 mm and +4 mm.

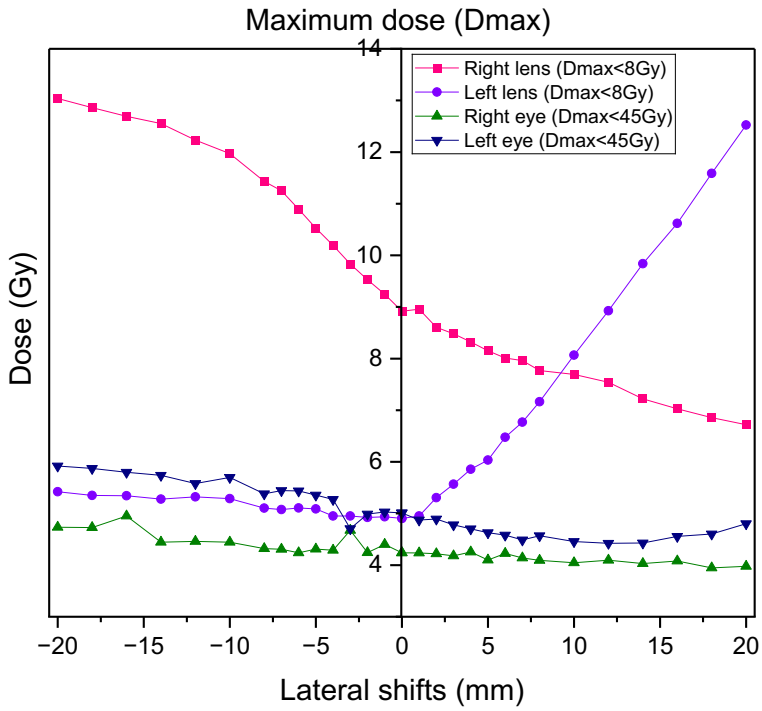

Figure 26: Impact of lateral shifts on maximum dose of surrounding eyes and lenses critical organs.

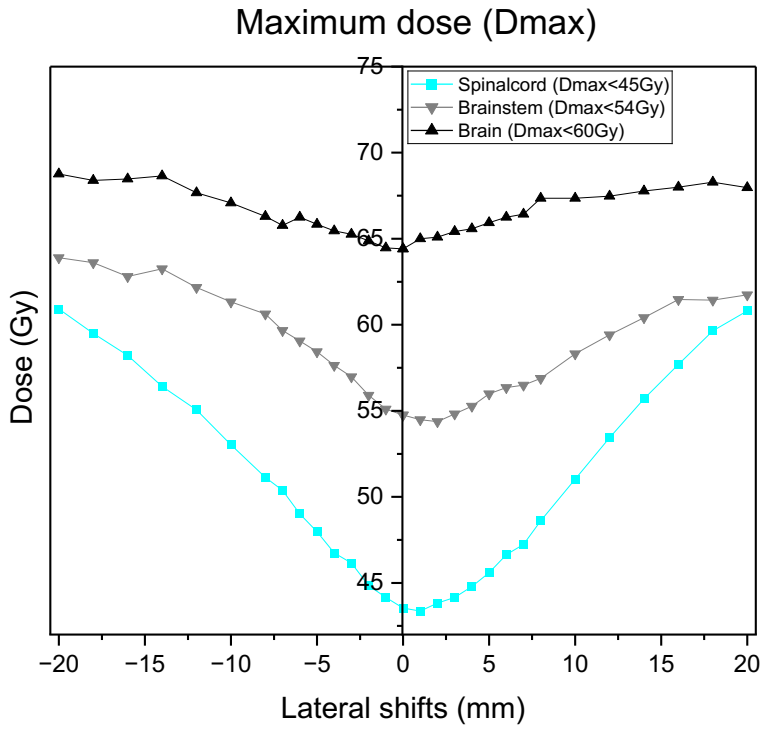

Figure 27: Impact of lateral shifts on maximum dose of surrounding spinal cord, brainstem, and brain critical organs.

4.3.2. Longitudinal shifts

The graphs presented in Figure 28-31 show the effects of longitudinal shifts on the dose distribution to both parotid glands, cochlear, spinal cord, brainstem, brain, lenses and eyes. The radiation dose to the right and left cochlear increases with superior shifts and decreases with inferior shifts, exceeding the 45 Gy constraint at +1 and +10 mm. The dose delivered to the parotid glands similarly increases with superior shifts and decreases with inferior shifts. For eyes and lenses, the left lens surpasses the 8 Gy constraint at +5 mm, and the right lens surpasses at 0 mm, while both eyes remain below the 45 Gy constraint even at -20 mm. The spinal cord, brain, and brainstem are highly sensitive to longitudinal shifts, with doses increasing for superior shifts and decreasing for inferior shifts.

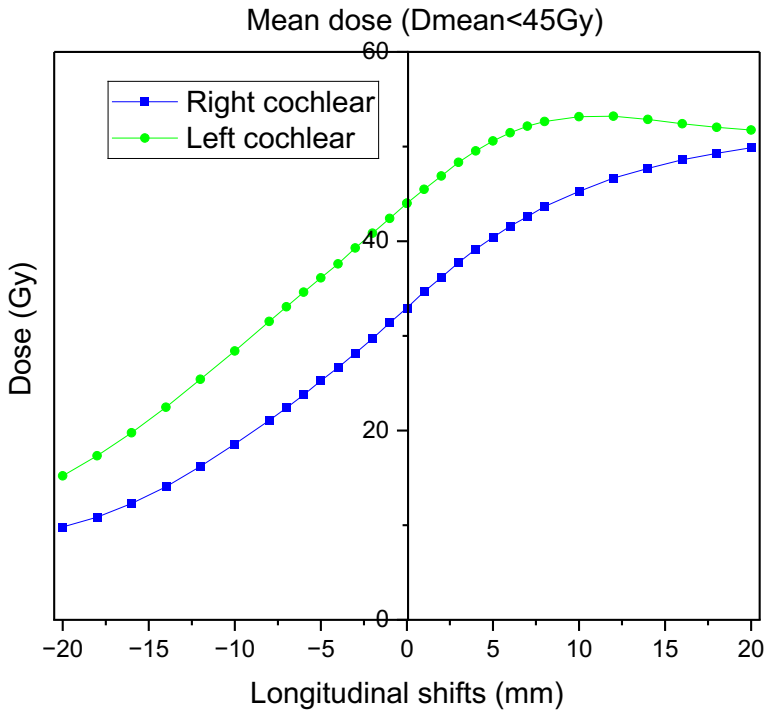

Figure 28: Impact of longitudinal shifts on mean dose of surrounding critical cochlear organs.

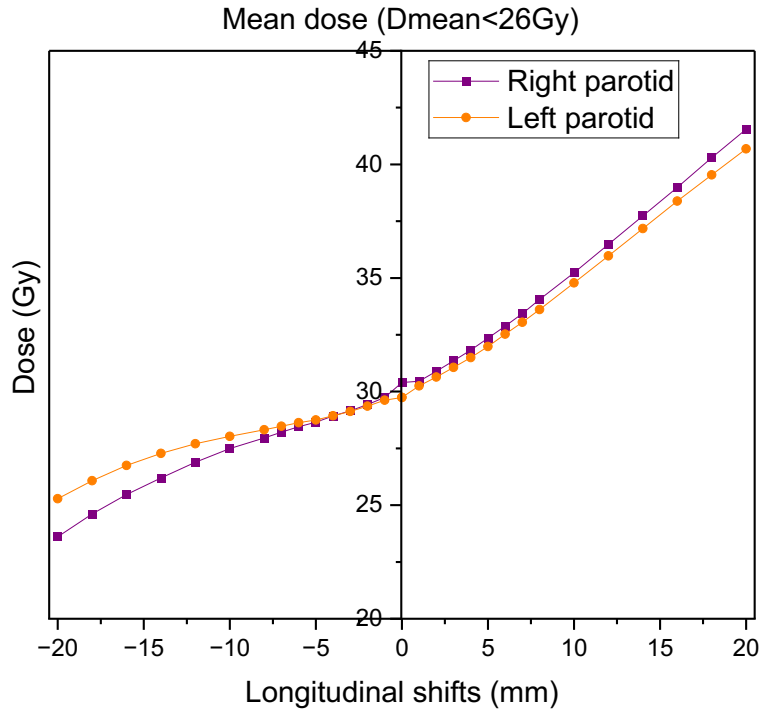

Figure 29: Impact of longitudinal shifts on mean dose of surrounding critical parotid glands.

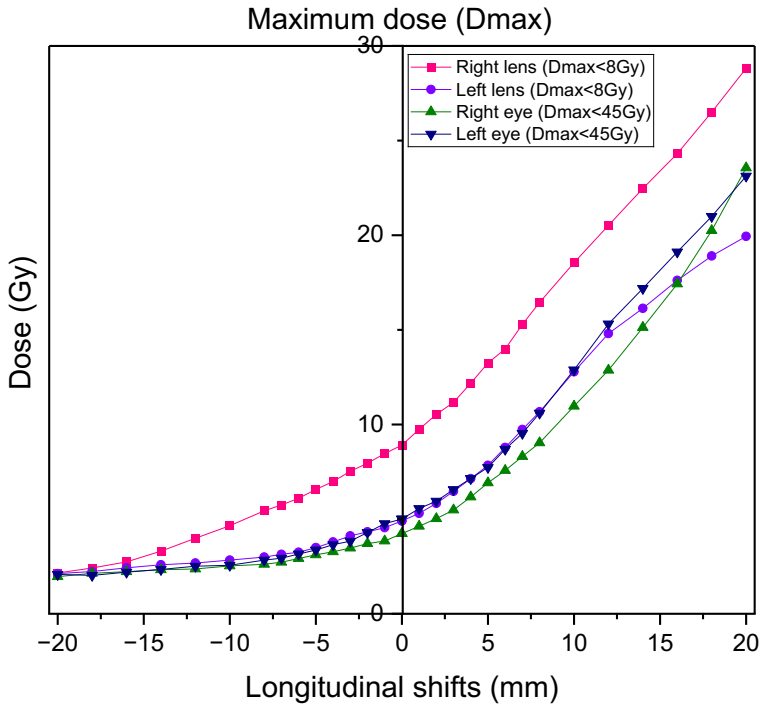

Figure 30: Impact of longitudinal shifts on maximum dose of surrounding critical organs, including eyes and lenses.

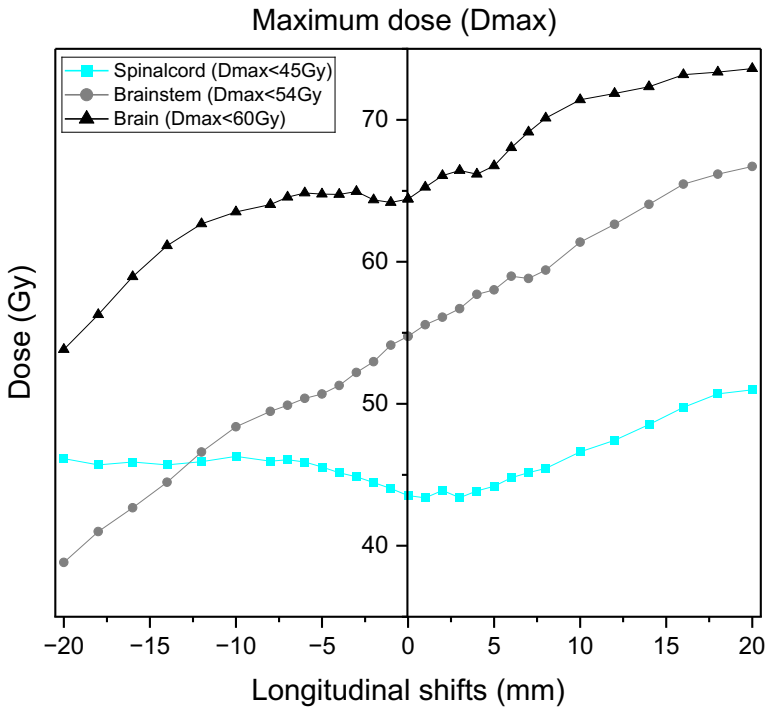

Figure 31: Impact of longitudinal shifts on maximum dose of surrounding critical organs, including spinal cord, brainstem, and brain.

4.3.3. Vertical shifts

Figures 32-35 illustrate the mean and maximum dose to critical structures, including the parotid glands, cochlear, spinal cord, brain, eyes, brainstem, and lenses, in response to posterior and anterior positional shifts. Vertical shifts impact the distribution of dose to critical organs. For the right and left cochlear, the dose increases with anterior shifts and decreases with posterior shifts. At -4 mm, the dose exceeds the 45 Gy constraint for left cochlear and right cochlear remains below the 45 Gy constraint even at maximum shifts of ±20 mm. The dose delivered to both parotid glands increases with posterior shifts and decreases slightly with anterior shifts. For the eyes and lenses, the right and left lens dose increases with posterior shifts and decreases with anterior shifts. While both eyes remain below the 45 Gy constraint across all directions, they are least affected by the shifts. The spinal cord, brainstem, and brain are highly sensitive to these shifts as they increase with anterior shifts and decline with posterior shifts. At -20 mm, the spinal cord, brainstem, and brain doses increase to approximately 70 Gy.

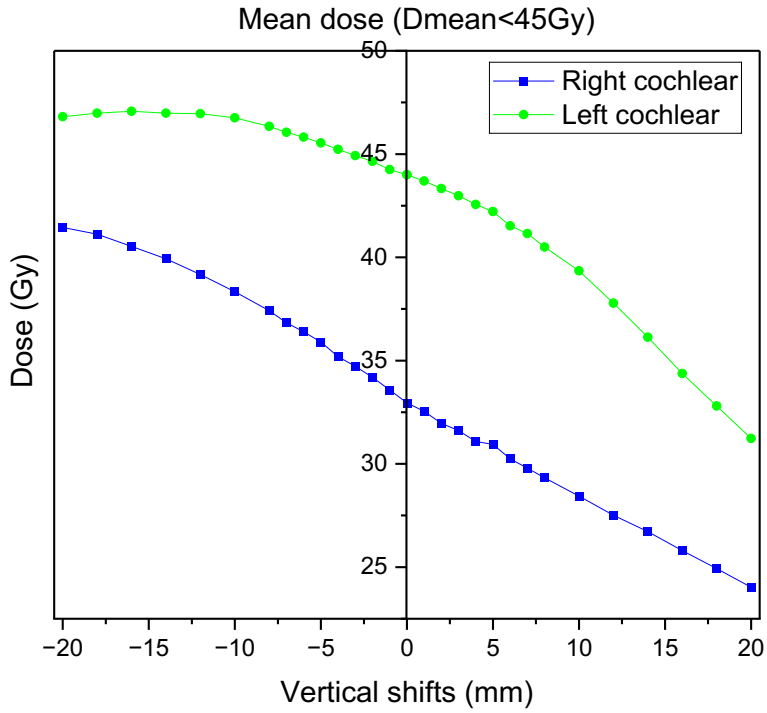

Figure 32: Impact of vertical shifts on mean dose of surrounding cochlear critical organs.

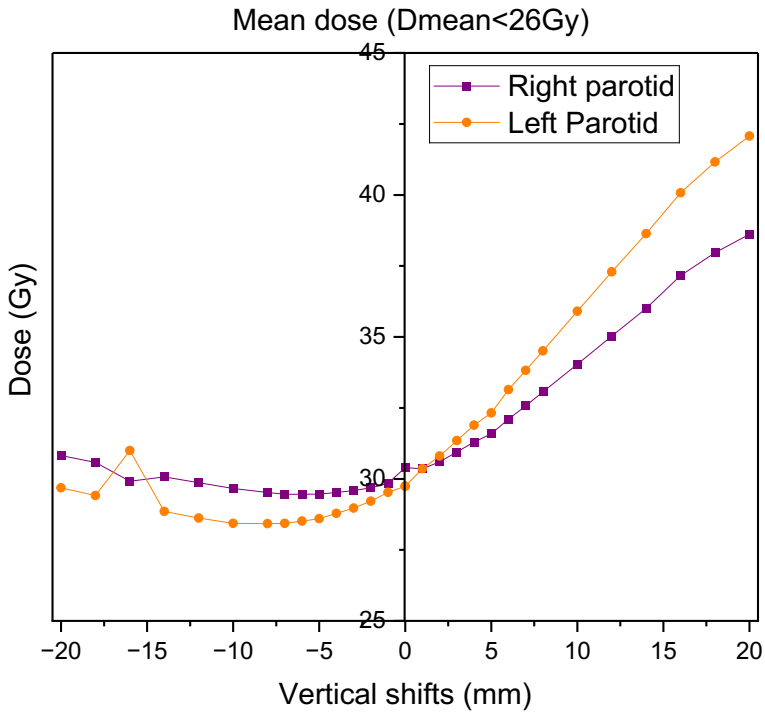

Figure 33: Impact of vertical shifts on mean dose of surrounding critical parotid glands.

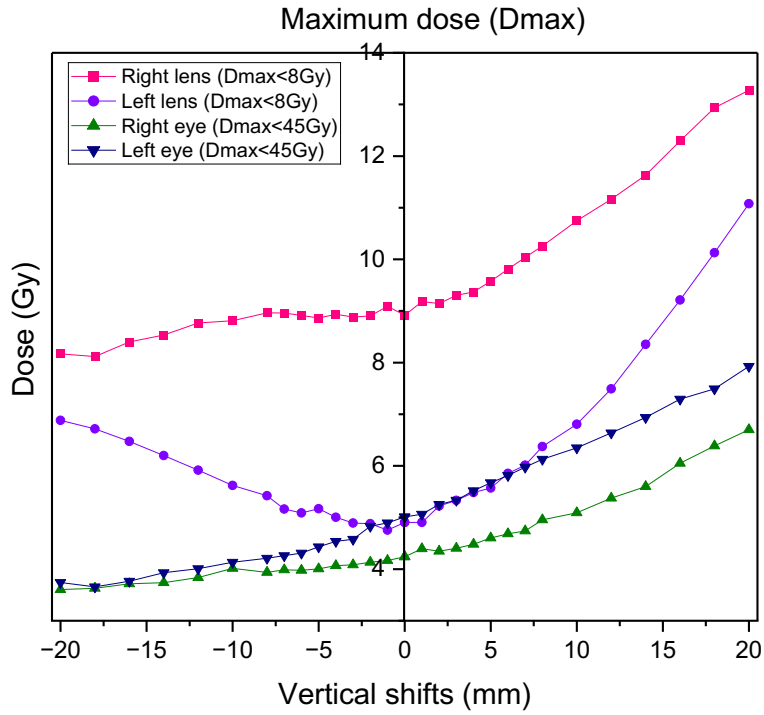

Figure 34: Impact of vertical shifts on maximum dose of surrounding eyes and lenses critical organs.

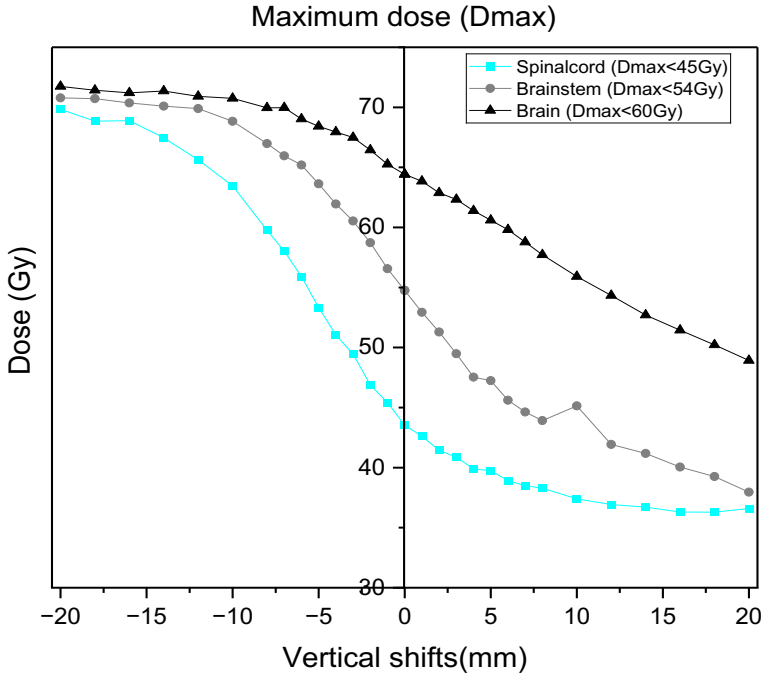

Figure 35: Impact of vertical shifts on maximum dose of surrounding critical organs like spinal cord, brainstem, and brain

4.5. OCTAVIUS 4D dose evaluation

This section presents results from PSQA measurement, giving the change of the gamma index, a measure of acceptable treatment delivery, with translation shifts. The PSQA graph shown in Figure 36 represents the effects of positional shifts on the gamma passing rate index of the radiotherapy plan from one of the patients. These translation shifts illustrate how isocenter shifts (used in this study as a reasonable indicator of setup errors) from the initial position affect the accuracy of the treatment delivery. In this study, a gamma criterion of 3%/3 mm was applied, where a dose difference of 3% and a 3 mm distance-to-agreement were required for a point to be considered passing. The gamma passing rate should not be less than 88% according to AAPM-TG-119 (Ezzell, et al., 2009). At CMJAH, a more stringent institutional gamma passing rate of 90% is applied, although plans with gamma passing rates as low as 88% may still be considered acceptable.

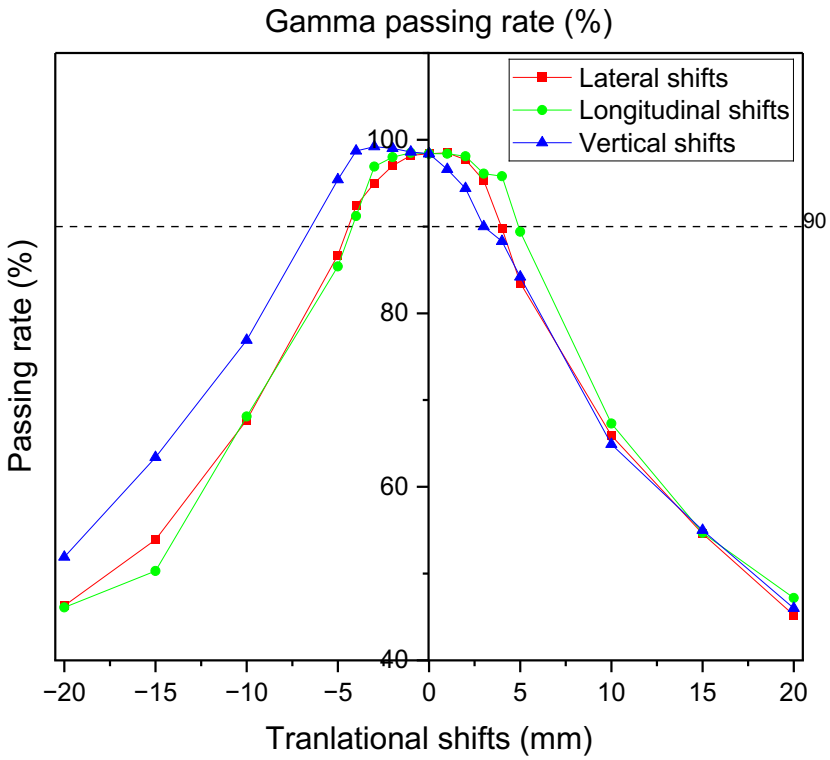

Figure 36: Impact of translational shifts; lateral (red), longitudinal (green), and vertical (blue) on gamma passing rate in PSQA.

Lateral shifts (red), both right and left, start with a 98.4% gamma passing rate at 0 mm and decrease passing rates as the shifts are introduced. For right lateral shifts, the passing rate decreases, failing at -5 mm, indicating a 5 mm shift tolerance, and continues to decrease to

46.3% at -20 mm. Similarly, left lateral shifts show the same trend, and with the passing rate failing at 4 mm, thus showing a 4 mm shift tolerance, and dropping to 45.2% at 20 mm, again suggesting that lateral shifts can degrade treatment accuracy.

Longitudinal shifts (shown in green), both inferior and superior, also start with a 98.5% gamma passing rate. These longitudinal shifts show a similar decrease in passing rates as lateral shifts, though the decrease is less than lateral shifts. For inferior shifts, the gamma passing rate decreases to 46.1% at -20 mm, while superior shifts also show a similar trend, decreasing to 47.2% at 20 mm. Both inferior and superior shifts show a shift tolerance of ±5 mm, suggesting that small positional errors in the longitudinal direction may be more acceptable than lateral shifts.

Vertical shifts, both anterior and posterior shifts, show a decrease in gamma passing rates. It decreases to 46.1% for anterior shifts at -20 mm, and its gamma passing rate fails at 6 mm, indicating a 6 mm shift tolerance. Posterior shifts show a similar decreasing trend, with the passing rate decreasing to 46% at 20 mm and showing a 4 mm shift tolerance since its passing rate fails at 4 mm.

Generally, the PSQA graph analysis shows that positioning accuracy is crucial in IGRT as it ensures high gamma passing rates. Lateral shifts decrease the passing rate more rapidly than longitudinal shifts, whereas vertical shifts impact the gamma passing rate most. Table 7 shows the shift tolerance in the PSQA for transitional shifts.

Table 5: Established shift tolerances obtained from measured PSQA data.

Translational shifts					
Lateral		Longitudinal		Vertical	
Rt lateral	Lt lateral	Inferior	Superior	Anterior	Posterior
5 mm	4 mm	5 mm	5 mm	6 mm	4 mm

Chapter 5

5. Conclusion

This research investigated the dosimetric impact of positional shifts on Shane phantom and nasopharynx cancer patients undergoing VMAT. The results show the effect of these shifts on the dose and the importance of patient positioning accuracy. They also show that an increase in positional shifts decreases the PTV dose, affecting both treatment effectiveness and the safety of critical organs.

The study's evaluation of the impact of positional shifts on PTV coverage and OAR exposure shows that high-dose PTVs (PTV_7000) are sensitive to positional errors; even minor positional shifts impact the dose, particularly when they exceed established shift tolerances of ±2 mm. Lower-dose PTVs (PTVn1_6000, PTVn2_5400) show larger shift tolerances and still show dose degradation beyond specific thresholds. Lateral and vertical shifts exhibit minimal asymmetry and have the exact shift tolerances of (2 mm), while longitudinal shifts were more relaxed towards the superior direction. These results are consistent with the accepted setup error tolerance or threshold of Hayder Alabedi (Alabedi, 2023), and indicate that posterior, inferior, and lateral shifts pose a greater risk of underdosing the PTV and potentially overdosing the surrounding critical organs.

The effect of positional shifts on the OAR dose for Shane phantom shows the need for patient positioning accuracy. The parotid glands were highly sensitive, exceeding dose constraints even with minor shifts, while the brainstem dose remained within the dose constraint and the spinal cord was least affected. Lateral and vertical shifts had the most impact, emphasizing the necessity for accurate patient positioning to prevent the risks of toxicity to the surrounding health organs. Patient data calculation confirms a similar trend to Shane phantom, with an established shift tolerance or threshold of 2 mm. Beyond these established shift tolerances, it results in PTV underdosing and OARs overdosing. These shifts also affected the hot spots, especially left lateral, superior, and posterior shifts, posing the risk of overdoing critical organs. The study shows the need for protocols that emphasize the need for accurate patient setup, daily IGRT, and enhanced immobilization devices to minimize the overdose of adjacent normal organs and underdose of the PTV, especially in nasopharyngeal cancer, where the proximity of surrounding organs requires accurate positioning.

PSQA data analysis illustrated the impact of positional shifts on gamma passing rates and helped establish shift tolerances for lateral, longitudinal, and vertical directions beyond which gamma passing rate fails, indicating compromised treatment accuracy. This highlights the need for accurate patient positioning and adherence to established shift tolerance or threshold, as large setup errors risk compromising the treatment outcome and increasing the risks of irradiating surrounding healthy tissues.

The observed translational setup errors in our research were ±2 mm in the x, y, and z axes, in line with some of the studies. Table 8 below illustrates the recommended positional shift tolerances and verification strategies in IGRT. In conclusion, this research shows that even minor setup errors can alter dose distribution, compromising the dose delivered to the PTV while increasing radiation exposure to adjacent organs. Rigorous verification techniques such as daily or weekly IGRT (e.g., CBCT), PSQA, and adaptive planning and regular use of QA tools like the Octavius® 4D system (PTW, Freiburg, Germany) are essential for maintaining treatment accuracy and effectiveness. Implementing strategies to control and correct setup errors is critical for effective tumour control.

Table 6: The summary of verification recommendations at CMJAH and literature comparison.

Aspect	Verification Recommended (CMJAH)	Literature Comparison
Primary Tolerances or threshold	±2 mm (Lateral), ±2 mm (Longitudinal), and ±2 mm (Vertical).	Hayder Alabedi (Alabedi, 2023) recommended ±2 mm shift tolerances for head and neck treatment to account for systematic errors and random errors.
Daily setup	Daily or Weekly CBCT/kV imaging is used to correct shifts exceeding the primary tolerance or threshold.	Tai et al. (Tai, et al., 2025) Recommended daily CBCT imaging in the head and neck region, essential for optimizing treatment outcomes.
Verification	Pre-treatment PSQA with gamma passing rate greater than 90% to ensure consistent and accurate treatment outcome	Ezzell et al. (Ezzell, et al., 2009) recommended gamma passing rate ≥ 88% (AAPM TG-119).
	Daily or Weekly CBCT imaging for anatomical changes and cumulative positional errors.	Tai et al. (Tai, et al., 2025) Recommended daily CBCT imaging in the head and neck region.
Adaptive planning	Re-plan for positional shifts beyond ±2 mm and anatomical changes, such as weight loss, which may compromise the effectiveness of immobilization devices like thermoplastic masks in the nasopharynx.	Mali Shrikant Balasaheb (Mali, 2016) highlight adaptive planning for anatomical changes such as weight loss affecting dose delivery.
Real-time imaging	It is important to monitor and correct shifts, although there is less organ movement in the nasopharynx.	Das et al. (Das, et al., 2024) Emphasizes daily imaging with kVCBCT or MV CBCT even in anatomical sites with minimal motion such as nasopharynx to enhance patient outcomes.

Chapter 6

6. References

O'Connor A., D., 1949. Radiographic checks of accuracy of application. *Br J Radiol,* 22(256), p. 206.

Li, G., Mageras, G., Dong, L. & Mohan, R., 2011. *Image-Guided Radiation Therapy.* 3rd Edition ed. Philadelphia, PA: Lippincott Williams & Wilkins.

Kataria, T., Abhishek, A., Chadha, P. & Nandigam, J., 2011. Set-up uncertainties: online correction with X-ray volume imaging. *Journal of Cancer Research and Therapeutics,* 7(1), p. 40–46.

Ling, C. C., Yorke, E. & Fuks, Z., 2006. From IMRT to IGRT: Frontier-land or neverland.. *Radiotherapy and Oncology,* Volume 78, pp. 119-122.

Goyal, S. & Kataria, T., 2014. Image Guidance in Radiation Therapy: Techniques and Applications. *Radiology Research and Practice.*

Bortfeld, T., 2006. IMRT: a review and preview. *Phys Med Biol,* 51(13), p. R363–R379.

Wu, Q. J., Li, T. & Yin, F. F., 2011. Adaptive radiation therapy: technical components and clinical applications. *Cancer Journal,* 17(3), p. 182–189.

Nijkamp, J., Pos, F. J., Nuver, T. T. & al., e., 2008. Adaptive radiotherapy for prostate cancer using kilovoltage cone-beam computed tomography: first clinical results. *Int J Radiat Oncol Biol Phys,* 70(1), p. 75–82.

FitzGerald, T. J., Urie, M., Ulin, K. & al., e., 2008. Processes for quality improvements in radiation oncology clinical trials. *Int J Radiat Oncol Biol Phys,* 71(1 Suppl), pp. S76-79.

Hartford, A. C., Palisca, M. G. & Eichler, T. J., 2009. American Society for Therapeutic Radiology and Oncology (ASTRO) and American College of Radiology (ACR) Practice Guidelines for Intensity-Modulated Radiation Therapy (IMRT). *Int J Radiat Oncol Biol Phys,* 73(1), pp. 9-14.

JAFFRAY, D. A., BISSONNETTE, J. -P. & CRAIG, T., 2005. *X-ray Imaging for Verification and Localization in Radiation Therapy", The Modern Technology of Radiation Oncology: A Compendium for Medical Physicists and Radiation Oncologists.* (VAN DYK, J., Ed.) ed. Madison, WI: Medical Physics Publishing.

Clements, M. et al., 2018. Monaco treatment planning system tools and optimization processes. *Medical Dosimetry,* 43(2), pp. 106-117.

INTERNATIONAL ATOMIC ENERGY AGENCY, 2013. *Record and Verify Systems for Radiation Treatment of Cancer: Acceptance Testing, Commissioning and Quality Control,* Vienna: IAEA Human Health Reports No. 7, IAEA.

Ramos, S. M. O., Thomas, S. & Berdeguez, M. B. T., 2017. Anthropomorphic phantoms-potential for more studies and training in radiology. *Int J Radiol Radiat Ther,* 2(4), pp. 101-104.

LAPOSTOLLE, P. M. & SEPT1ER, A. L., 1970. *(Eds), Linear Accelerators,* Amsterdam: North-Holland Publishing Co..

KARZMARK, C. J. & PERING, N. C., 1973. Electron linear accelerators for radiation therapy: history, principles and contemporary developments. *Phys. Med. Biol.,* 18(3), p. 321.

ALMOND, P. R., 1975. Some applications of particle accelerators to cancer research and treatment. *Phys. Rep.,* 17(1), pp. 1-35.

Feldkamp, I. A., Davis, L. C. & Kress, J. W., 1984. Practical cone-beam algorithm. *J Opt Soc Am A,* 1(6), pp. 612-619.

Barry, A., Loredana, M. & Eva, B., 2012. *Biomedical physics in radiotherapy for cancer.* 1st ed. Collingwood (VIC): CSIRO Publishers.

Herman, M. G., 2005. Clinical use of electronic portal imaging. *Seminars in Radiation Oncology,* 15(3), p. 157–167.

Van Herk, M., 2004. Errors and margins in radiotherapy. *Seminars in Radiation Oncology,* 14 (1), p. 52–64.

Bel, A., Van Herk, M., Bartelink, H. & Lebesque, J. V., 1993. A verification procedure to improve patient set-up accuracy using portal images. *Radiotherapy and Oncology,* 29(2), p. 253–260.

Rasch, C., Steenbakkers, R. & and Van Herk, M., 2005. Target definition in prostate, head, and neck. *Seminars in Radiation Oncology,* 15(3), p. 136–145.

Mukherji, S. K. & Miracle, A. C., 2009. Conebeam CT of the head and neck, Part 2: clinical applications. *Am J Neuroradiol,* 30(7), p. 1285–1292.

Jaffray, D. A., 2007. Kilovoltage volumetric imaging in the treatment room. *Frontiers of Radiation Therapy and Oncology,* Volume 40, p. 116–131.

McBain, et al., 2006. X-ray volumetric imaging in image-guided radiotherapy: the new standard in on-treatment imaging. *International Journal of Radiation Oncology, Biology, Physics,* 64(2), p. 625–634.

Morin, O., Gillis, A., Chen, J. & et al., 2006. Megavoltage cone-beam CT: system description and clinical applications. *Medical Dosimetry,* 31(1), p. 51–61.

Jaffray, D. A. & Wong, J. W., 2013. Image-guided radiation therapy: a new era of precision in radiation oncology. *Nature Reviews Cancer,* 13(7), pp. 499-509.

Pouliot, J., Bani-Hashemi, A., Svatos, M. & et al., 2005. Low-dose megavoltage cone-beam CT for radiation therapy. *International Journal of Radiation Oncology Biology Physics,* 61(2), p. 552–560.

Antonuk, L. E. et al., 1996. Megavoltage imaging with a large-area, flat-panel, amorphous silicon imager. *Int J Radiat Oncol Biol Phys.,* 36(3), pp. 661-672.

Antonuk, L. E., Boudry, J., Huang, W. D. & al., e., 1993. Demonstration of megavoltage and diagnostic-x-ray imaging with hydrogenated amorphous-silicon arrays. *Med Phys.,* 19(6), pp. 1455-1466.

Herman, M. G., Balter, J. M., Jaffray, D. A. & al., e., 2001. Clinical use of electronic portal imaging: report of AAPM Radiation Therapy Committee Task Group 58. *Med Phys.,* 28(5), pp. 712-737.

Essers, M. et al., 1996. Transmission dosimetry with a liquid-filled electronic portal imaging device. *Int J Radiat Oncol Biol Phys.,* 34(4), pp. 931-941.

Kirby, M. C. & Williams, P. C., 1995. The use of an electronic portal imaging device for exit dosimetry and quality-control measurements. *Int J Radiat Oncol Biol Phys.,* 31(3), pp. 593-603.

Herman, M. G. et al., 2001. Clinical use of electronic portal imaging: Report of AAPM Radiation Therapy Comittee Task Group 58. *Medical Physics,* 28(5), p. 71.

Shen, A. & and Luo, L., 2008. *Point-based digitally reconstructed radiograph,* Los Alamitos, CA, USA: IEEE.

Dorgham, O., Fisher, M. & Laycock, S., 2009. Accelerated generation of digitally reconstructed radiographs using parallel processing. *In Proc. Medical Image Understanding and Analysis,* pp. 14-15.

Nagata, Y. et al., 1990. CT simulator: A new 3-D planning and simulation system for radiotherapy: Part 2. Clinical application. *Int. J. Radiat. Oncol. Biol. Phys.,* Volume 18, pp. 505-513.

Serrurier, A., Bönsch, A., Lau, R. & Deserno, T. M., 2015. MRI visualisation by digitally reconstructed radiographs. *In Medical Imaging 2015: PACS and Imaging Informatics: Next Generation and Innovations,* Volume 9418, pp. 102-108.

Markelj, P. & et al., 2012. A review of 3D/2D registration methods for image-guided interventions. *Medical Image Analysis,* 16(3), pp. 642-661.

Jaffray, D., Kupelian, P., Djemil, T. & Macklis, R., 2007. Review of imageguided radiation therapy. *Exp Rev Anticancer Ther.,* 7(1), pp. 89-103.

Li, G., Mageras, G., Dong, L. & Mohan, R., 2011. *Image-Guided Radiation Therapy.* 3rd ed. Philadelphia, PA: Lippincott Williams & Wilkins.

Kim, J., Jin, J. Y., Walls, N. & al., e., 2011 . Image-guided localization accuracy of stereoscopic planar and volumetric imaging methods for stereotactic radiation surgery and stereotactic body radiation therapy: a phantom study. *Int J Radiat Oncol Biol Phys.,* 79(5), pp. 1588-1596.

Peng, L. C., Kahler, D., Samant, S. & al., e., 2010. Quality assessment of frameless fractionated stereotactic radiotherapy using cone beam computed tomography. *Int J Radiat Oncol Biol Phys.,* 78(5), pp. 1586-1593.

Sun, H., 2023. A Review of 3D-2D Registration Methods and Applications based on Medical Images. *Highlights in Science, Engineering and Technology,* Volume 35, p. 200–224.

Teoh, M. et al., 2011. Volumetric modulated arc therapy:A review of current literature and clinical use in practice. *Br J Radiol.,* 84(1007), p. 967–996.

Oliver, M., Ansbacher, W. & Beckham, W. A., 2009. Comparing planning time delivery time and plan quality for IMRT, rapidarc and tomotherapy. *J Appl Clin Med Phys.,* 10(4), p. 117–131.

Macchia, G. et al., 2017. Volumetric modulated arc therapy for treatment of solid tumors: current insights. *Onco Targets Ther.,* Volume 10, pp. 3755-3772.

ICRU, 2010. *Prescribing, Recording, and Reporting Photon-Beam Intensity-Modulated Radiation Therapy (IMRT),* Oxford, UK: ICRU Report 83, J. ICRU, Volume 10(1). Oxford University Press.

ICRU, 1993. *Prescribing, recording and reporting photon beam therapy,* Bethesda: ICRU report 50; ICRU publications.

ICRU, 1999. *Prescribing, recording, and reporting photon beam therapy,* Bethesda (MD): ICRU Report 62; Measurements ICoRUa.

ICRU, 1994. *Prescribing, recording and reporting photon beam therapy,* Bethesda (MD): In ICRU Report 50; ICRU Publications.

ICRU, 2000. *Prescribing, recording and reporting photon beam therapy (Supplement to ICRU report 50),* Bethesda (MD): In ICRU Report 62; ICRU Publications.

Langmack, K. A., 2001. Portal imaging. *The British journal of radiology,* 74(885), pp. 789-804.

Marks, L. B. et al., 2010. Use of normal tissue complication probability models in the clinic. *International Journal of Radiation Oncology Biology Physics,* 76(3.), pp. S10-S9.

Grills, I. S. et al., 2007. Image guided radiotherapy (IGRT) via online cone beam CT substantially reduces margin requirements for stereotactic lung radiotherapy. *Int J Radiat Oncol,* 69(3), p. S154.

Urso, P. et al., 2018. Practical application of Octavius® -4D: Characteristics and criticalities for IMRT and VMAT verification. *J Appl Clin Med Phys.,* Sep, 19(5), pp. 517-524.

Morsy, M. A., Ahmed, A. R. & Elshahat, K. M., 2019. Measure the Errors of Treatment Set-Ups of Prostate Cancer Patient Using Electronic Portal Imaging Device (EPID). *IOSR Journal of Applied Physics,* 10(2), pp. 55-59.

Rahman, H. et al., 2023. A Systematic Literature Review of 3D Deep Learning Techniques in Computed Tomography Reconstruction. *Tomography,* 9(6), pp. 2158-2189.

Purdy, A., 2008. Dose to normal tissues outside the radiation therapy patient's treated volume: a review of different radiation therapy techniques. *Health Phys.,* 95(5), p. 666–676.

Cannon, D. M. & Lee, N. Y., 2008. Recurrence in region of spared parotid gland after definitive intensity-modulated radiotherapy for head and neck cancer. *International Journal of Radiation Oncology* Biology* Physics,* 70(3), pp. 660-665.

Chen, A. M. et al., 2011. Marginal misses after postoperative intensity-modulated radiotherapy for head and neck cancer. *International Journal of Radiation Oncology* Biology* Physics,* 80(5), pp. 1423-1429.

Macchia, G. et al., 2017. Volumetric modulated arc therapy for treatment of solid tumors: current insights. *Onco Targets Ther.,* Volume 10, p. 3755–3772.

Barber, J. et al., 2017. A survey of modulated radiotherapy use in Australia & New Zealand in 2015. *Australas Phys Eng Sci Med.,* 40(4), pp. 811-822.

Peng, J. et al., 2020. A Comparison of Radiation Techniques in Patients Treated With Concurrent Chemoradiation for Stage III Non-Small Cell Lung Cancer. *Int J Radiat Oncol Biol Phys.,* 106(5), pp. 985-992.

Kazantsev, P. et al., 2019. 'IAEA methodology for on-site end-to-end IMRT/VMAT audits: an international pilot study'. *Acta Oncologica,* 59(2), p. 141–148.

Hall, E. J. & Giaccia, A. J., 2019. *Radiobiology for the radiologist.* 8th ed. Philadelphia, PA: Wolters Kluwer.

Zhao, Y. et al., 2020. Impact of Positioning Errors on the Dosimetry of Breath-Hold-Based Volumetric Arc Modulated and Tangential Field-in-Field Left-Sided Breast Treatments. *Front. Oncol. ,* 10(554131).

Alabedi, H., 2023. Assessing setup errors and shifting margins for planning target volume in head, neck, and breast cancer. *J Med Life,* 16(3), pp. 394-398.

Ezzell, G. A. et al., 2009. IMRT commissioning: multiple institution planning and dosimetry comparisons, a report from AAPM Task Group 119.. *Med Phys.,* 36(11), pp. 5359-73..

Zhou, X. et al., 2024. Current state, challenges, and future perspective of adaptive radiotherapy: A narrative review of nasopharyngeal carcinoma.. *Oral Oncol.,* 58(107008).

Du, T., Xiao, J., Qiu, Z. & Wu, K., 2019. The effectiveness of intensity-modulated radiation therapy versus 2D-RT for the treatment of nasopharyngeal carcinoma: A systematic review and meta-analysis. *PLoS One,* 14(7).

Zhu, F., Wu, Y. & & Wang, H., 2023. Advance in integrating platinum-based chemotherapy with radiotherapy for locally advanced nasopharyngeal carcinoma. *Frontiers in Oncology,* Volume 13..

Ng, W. T. et al., 2022. Current Radiotherapy Considerations for Nasopharyngeal Carcinoma. *Cancers (Basel),* 14(23), p. 5773.

Breitkreutz, D. Y., Weil, M. D. & M., B.-C., 2020. External beam radiation therapy with kilovoltage x-rays. *Physica Medica: European Journal of Medical Physics,* Volume 79, pp. 103 - 112.

Luchka, K. et al., 1996. Assessing radiation and light field congruence with a video based electronic portal imaging device. *Med Phys.,* 23(7), pp. 1245-1252.

Xu, F. et al., 2008. Interfractional and intrafractional setup errors in radiotherapy for tumors analyzed by cone-beam computed tomography. *Ai Zheng= Aizheng= Chinese Journal of Cancer,* 27(10), pp. 1111-1116.

Li, X. A. et al., 2007. Interfractional variations in patient setup and anatomic change assessed by daily computed tomography. *International Journal of Radiation Oncology* Biology* Physics,* 68(2), pp. 581-591..

Malan, D. F., van der Walt, S. J., Raidou, R. G. & al., e., 2016. A fluoroscopy-based planning and guidance software tool for minimally invasive hip refixation by cement injection. *Int J CARS,* Volume 11, p. 281–296.

Srinivasan, K., Mohammadi, M. & Shepherd, J., 2014. Applications of linac-mounted kilovoltage Cone-beam Computed Tomography in modern radiation therapy: A review. *Pol J Radiol.,* Volume 79, pp. 181-93.

Yeh, C.-Y., Lai, P.-A., Liu, F.-H. & & He, C.-C., 2023. Fractionated Volumetric Modulated Arc Therapy (FVMAT) for Oligometastatic Brain Tumor. *Onco. ,* 3(1), pp. 43-52. .

Stroom, J. C. & Heijmen, B. J., 2002. Geometrical uncertainties, radiotherapy planning margins, and the ICRU-62 report. *Radiother Oncol.,* 64(1), pp. 75-83.

El-Shahat, K., Salem, M., Ali, A. & El-Taher, A., 2023. The Influence of Electronic Portal Imaging Devices (EPIDs) used in Radiotherapy: Image Quality and Dose Measurements. *Journal of Radiation and Nuclear Applications,* 8(3), p. 237.

Berlin, L., 2014. Reviewing the CT scout view: medicolegal and ethical considerations. *AJR Am J Roentgenol.,* 202(6), pp. 1264-6.

Peng, C., Morrow, N., Lawton, C. & Li, X., 2009. Advantages of Diagnostic Quality CT Guided Radiotherapy for Prostate Cancer: Margin Reduction and Dose Escalation. *International Journal of Radiation Oncology, Biology, Physics,* 75(3), p. 631.

Murphy, M. J. et al., 2007. The management of imaging dose during image-guided radiotherapy: report of the AAPM Task Group 75. *Med Phys.,* 34(10), pp. 4041-63.

Seravalli, E. et al., 2024. Surface guided radiotherapy practice in paediatric oncology: a survey on behalf of the SIOPE Radiation Oncology Working Group. *Br J Radiol.,* 97(1157), pp. 1044-1049.

Kord, M. et al., 2021. Risks and Benefits of Fiducial Marker Placement in Tumor Lesions for Robotic Radiosurgery: Technical Outcomes of 357 Implantations. *Cancers (Basel),* 13(19), p. 4838.

Vassileva, J., 2025. *Patient dose in image-guided radiotherapy (IGRT),* Ottawa: International Commission on Radiological Protection.

Tai, D. T. et al., 2025 . Enhancing patient positioning accuracy: evaluating daily cone beam computed tomography in the halcyon system. *Jpn J Clin Oncol.,* 55(8), pp. 925-932.

Mali, S. B., 2016. Adaptive Radiotherapy for Head Neck Cancer. *J Maxillofac Oral Surg.,* 15(4), pp. 549-554.

Das, P. et al., 2024. Precision in Delivery: The Critical Role of Daily Imaging in Radiotherapy for Nasopharyngeal Cancer with VMAT Technique. *Asian Pacific Journal of Cancer Care,* 9(4), pp. 901-904.